NOTICE

The quality of this microform is heavily dependent upon the quality of the original thesis submitted for microfilming. Every effort has been made to ensure the highest quality of reproduction possible.

If pages are missing, contact the university which granted the degree.

Some pages may have indistinct print especially if the original pages were typed with a poor typewriter ribbon or if the university sent us an inferior photocopy.

Reproduction in full or in part of this microform is governed by the Canadian Copyright Act, R.S.C. 1970, c. C-30, and subsequent amendments.

AVIS

La qualité de cette microforme dépend grandement de la qualité de la thèse soumise au microfilmage. Nous avons tout fait pour assurer une qualité supérieure de reproduction.

S'il manque des pages, veuillez communiquer avec l'université qui a conféré le grade.

La qualité d'impression de certaines pages peut laisser à désirer, surtout si les pages originales ont été dactylographiées à l'aide d'un ruban usé ou si l'université nous a fait parvenir une photocopie de qualité inférieure.

La reproduction, même partielle, de cette microforme est soumise à la Loi canadienne sur le droit d'auteur, SRC 1970, c. C-30, et ses amendements subséquents.

Propagation of Transients in Dispersive Dielectric Media

by
Man Duc Bui

A thesis submitted to
the School of Graduate Studies and Research
in partial fulfillment of the requirements
for the degree of
Master of Applied Science

Ottawa-Carleton Institute for Electrical Engineering
Department of Electrical Engineering
Faculty of Engineering
University of Ottawa

ISBN 0-315-60023-3

UNIVERSITÉ D'OTTAWA
UNIVERSITY OF OTTAWA

I hereby declare that I am the sole author of this document. I authorize the University of Ottawa to lend this document to other institutions or individuals for the purpose of scholarly research.

Man D. Bui

I further authorize the University of Ottawa to reproduce this document by photocopying or by other means, in total or in part, at the request of other institutions or individuals for the purpose of scholarly research.

Man D. Bui

Abstract

Propagation of transient electromagnetic fields in dispersive dielectric media is studied. The dielectric medium is assumed to be linear, isotropic, and homogeneous and is described by the Debye model. Incident fields are assumed to be TEM plane wave pulses. The dielectric can assume the form of infinite half space or infinite circular cylinder; either of which may be homogeneous or stratified. The electric fields induced in the dielectric are calculated from Time Domain Maxwell's equations using Finite Difference Time Domain method. The results of this investigation can be used for geophysical probing, subsurface communication and for investigating possible biological effects of pulsed electromagnetic fields.

Acknowledgements

The author is greatly indebted to Professors S.S. Stuchly and G. Costache, his thesis co-supervisors, for their guidance and constant encouragement throughout this work. It is a pleasure to thank all the graduate students with whom the author had many stimulating discussions. The use of the computing facilities at the University of Ottawa is also acknowledged.

The work reported in this thesis was supported by the Natural Science and Engineering Research Council of Canada.

Contents

List of Figures

Chapter 1

Introduction

1.1 Motivation

The ever increasing use of electromagnetic devices has led to mounting concern about the biological effects and potential hazards of electromagnetic radiation. Most of the research in biological effects of electromagnetic radiation has been done with continuous-wave radiation [1] [2]. Although there has been concern over the hazards of pulsed radiation [2] [3], little work has been done about it. Most of the work done with pulsed-wave radiation did not include the dispersive dielectric properties of biological materials.

In addition, there has been an interest in the propagation of transient electromagnetic waves through lossy dispersive dielectrics related to its applications in important real problems such as geophysical probing and subsurface studies of the moon and other planets [4] [5] [6] [7].

Thus, there is a need for investigating the propagation of pulses into lossy dispersive materials for developing suitable models of the human body and geological structures.

1.2 Objective

The objective of this work is to investigate the propagation of pulsed electromagnetic fields in dispersive dielectrics.

The dielectric is assumed to be linear, isotropic, and homogeneous and is described by the Debye model [31]. Incident fields are assumed to be TEM

(transverse electromagnetic) plane wave pulses. The dielectric can assume the form of infinite half space or infinite circular cylinder; either of which may be homogeneous or stratified.

The electric fields induced in the dielectric are calculated from time domain Maxwell's equations using Finite-Difference Time-Domain method.

1.3 Present State of Knowledge

Transient fields in dispersive media have been the subject of a number of investigations.

Some authors used analytical approximation techniques to study pulse propagation problems. Wait [8] studied the distortion of a pulse propagating through a dispersive medium using various approximate procedures based on stationary phase principle. Fuller and Wait [4] calculated the unit-step impulse response for a compound Debye dielectric model by taking the Laplace Transform of the transfer function and then approximating the propagation constant for short and long time behaviors.

Other authors studied the problem in the frequency domain. Sivaprasad *et al.* [9] studied the reflection for a sine-squared pulse incident at normal and oblique angles on a three-layer medium with the middle layer being a Debye dielectric. Suzuki *et al.* [6] obtained the waves reflected by two dielectric slabs for an incident pulse-modulated carrier wave analytically by expanding the reflection coefficient of an elementary plane wave into a series expansion. Bussey and Richmond [10] obtained a theoretical scattering solution in the frequency domain for a plane wave incident normally on a lossy dielectric multilayer circular cylinder of infinite length by assuming the solution to be in the form of a Fourier series of Bessel functions of first and second kinds.

Still other authors evaluated the steady-state transfer-function as a function of frequency. King and Harrison [5] studied the transmission of an incident pulse of Gaussian shape from the air into the earth by evaluating the steady-state transfer function over a frequency spectrum. Lin [11] studied the interaction of electromagnetic transient radiation with biological materials by developing a steady state transfer function at the interface of air and a Debye medium. Lin *et al.* [12] [13] also determined the transmitted field strengths in homogeneous spherical models of human and animal heads by convolving the Fourier transform of the incident pulse with the steady-state

transfer function of the medium. The transmitted pulse in the time domain was then obtained by an inverse Fourier transformation.

Durney *et al.* [14] [15] used Fourier Series Expansion technique to expand the incident pulse train into a Fourier series to study the propagation of wave in a dispersive dielectric half space irradiated by an electromagnetic plane wave pulse train.

Very few authors studied the problem directly in the time domain. Lam [16] investigated the reflected waveform of a unit-step signal incident on a Debye dielectric half space and on an ice layer on water using an integro-differential equation which was solved numerically by Finite Difference Time Domain method. Bolomey *et al.* [17] studied the reflected field at the interface of a Debye medium illuminated by a ramp incident field from the air using Time Domain Integral Equation. Holland *et al.* [18] and Sullivan *et al.* [19] used the Finite Difference Time-Domain method to calculate the electric field and the SAR (Specific Absorption Rate) distribution in a model of the human body. The dielectric was assumed to be nondispersive.

Chapter 2

Theory

2.1 Introduction

In this chapter, we shall discuss in detail the Finite Difference Time Domain method (FDTD method) for solution of the Time Domain Maxwell's equations in Debye media. We shall start from the examination of the Time Domain Maxwell's equations in a Debye medium and derive the expressions for the electric flux density and its first and second derivatives with respect to time. We shall then derive the numerical solution of the Time Domain Maxwell's equations for one and two-dimensional problems. We shall also investigate the boundary conditions at the interface of two different media in order to be able to treat the pulse propagation in inhomogeneous media.

2.2 Time Domain Maxwell's Equations in a Debye Medium

Source-free Time Domain Maxwell's equations are:

$$\nabla \times \vec{E}(x,y,z,t) = -\frac{\partial \vec{B}(x,y,z,t)}{\partial t} \tag{2.1}$$

$$\nabla \times \vec{H}(x,y,z,t) = \frac{\partial \vec{D}(x,y,z,t)}{\partial t} + \sigma \vec{E}(x,y,z,t) \tag{2.2}$$

where $\vec{B}(t)$ and $\vec{D}(t)$ are the inverse Fourier transforms of $\vec{\mathcal{B}}(\omega)$ and $\vec{\mathcal{D}}(\omega)$ which are defined in the frequency domain:

$$\vec{\mathcal{B}}(\omega) = \mu^*(\omega)\vec{\mathcal{H}}(\omega) \tag{2.3}$$

$$\vec{\mathcal{D}}(\omega) = \epsilon^*(\omega)\vec{\mathcal{E}}(\omega) \tag{2.4}$$

The unknowns are the electric field $\vec{E}(t)$, and the magnetic field $\vec{H}(t)$. The medium is assumed homogeneous and isotropic within each layer.The permeability is that of free space μ_0. The conductivity σ is constant. The permittivity is assumed the form of Debye model with a single relaxation time:

$$\epsilon^*(\omega) = \epsilon_\infty + \frac{\epsilon_0 - \epsilon_\infty}{1 + j\tau_0\omega} \tag{2.5}$$

where ϵ_0 and ϵ_∞ are the low and high frequency permittivities, respectively, and τ_0 is the relaxation time.

Taking the Inverse Fourier Transform of (2.5), (2.3) and (2.4), one obtains $\epsilon(t)$, $\vec{B}(t)$ and $\vec{D}(t)$:

$$\begin{aligned}
\epsilon(t) &= \epsilon_\infty\delta(t) + \frac{\epsilon_0 - \epsilon_\infty}{\tau_0}e^{-\frac{t}{\tau_0}}u(t) \\
\vec{B}(t) &= \mu_0\vec{H}(t) \\
\vec{D}(t) &= \int_{-\infty}^{\infty} \epsilon(t-\beta)\vec{E}(\beta)d\beta\,.
\end{aligned}$$

Therefore, the electric flux density is:

$$\vec{D}(t) = \epsilon_\infty\vec{E}(t) + \frac{\epsilon_0 - \epsilon_\infty}{\tau_0}\int_{-\infty}^{\infty} e^{-\frac{t-\beta}{\tau_0}}u(t-\beta)\vec{E}(\beta)d\beta\,.$$

Suppose we write:

$$\vec{D} = D_x\vec{x} + D_y\vec{y} + D_z\vec{z}\,,$$

then:

$$D_x(t) = \epsilon_\infty E_x(t) + \frac{\epsilon_0 - \epsilon_\infty}{\tau_0}\int_{-\infty}^{\infty} e^{-\frac{t-\beta}{\tau_0}}u(t-\beta)E_x(\beta)d\beta\,.$$

By differentiating the above equation twice with respect to t (see Appendix A for details), we obtain the first and second derivatives of $D_x(t)$:

$$\frac{\partial D_x(t)}{\partial t} = \epsilon_\infty \frac{\partial E_x(t)}{\partial t} + \frac{\epsilon_0 - \epsilon_\infty}{\tau_0}\left[E_x(t) - \frac{\Delta t}{\tau_0} S_x(t)\right] \tag{2.6}$$

$$\frac{\partial^2 D_x(t)}{\partial t^2} = \epsilon_\infty \frac{\partial^2 E_x(t)}{\partial t^2} + \frac{\epsilon_0 - \epsilon_\infty}{\tau_0}\left[\frac{\partial E_x(t)}{\partial t} - \frac{1}{\tau_0} E_x(t) + \frac{\Delta t}{\tau_0^2} S_x(t)\right] \tag{2.7}$$

where

$$S_x(t) = \frac{1}{\Delta t} \int_{-\infty}^{\infty} e^{-\frac{t-\beta}{\tau_0}} u(t-\beta) E_x(\beta) d\beta \,,$$

and Δt is the time increment.

The lower integration limit can be changed to 0 because of the causality of the fields, and the upper integration limit can be changed to t by omitting the unit-step function $u(t-\beta)$ in the integrand. Thus we can rewrite $S_x(t)$ as:

$$S_x(t) = \frac{1}{\Delta t} \int_0^t e^{-\frac{t-\beta}{\tau_0}} E_x(\beta) d\beta \,. \tag{2.8}$$

To reduce the integral to a recursive form, we split it into two parts:

$$S_x(t) = \frac{1}{\Delta t} \int_0^{t-\Delta t} e^{-\frac{t-\beta}{\tau_0}} E_x(\beta) d\beta + \frac{1}{\Delta t} \int_{t-\Delta t}^{t} e^{-\frac{t-\beta}{\tau_0}} E_x(\beta) d\beta$$

We then integrate the second integral from $t-\Delta t$ to t by using the trapezoidal rule [16] so that:

$$S_x(t) = \frac{1}{\Delta t} \int_0^{t-\Delta t} e^{-\frac{t-\Delta t-\beta+\Delta t}{\tau_0}} E_x(\beta) d\beta + \frac{1}{2}\left[e^{-\frac{\Delta t}{\tau_0}} E_x(t-\Delta t) + E_x(t)\right]$$

and then by removing a constant $e^{-\frac{\Delta t}{\tau_0}}$ outside the integral sign and substituting the integral with (2.8), we get:

$$S_x(t) = \frac{e^{-\frac{\Delta t}{\tau_0}}}{\Delta t} \int_0^{t-\Delta t} e^{-\frac{t-\Delta t-\beta}{\tau_0}} E_x(\beta) d\beta + \frac{1}{2}\left[e^{-\frac{\Delta t}{\tau_0}} E_x(t-\Delta t) + E_x(t)\right] \,,$$

and

$$S_x(t) = e^{-\frac{\Delta t}{\tau_0}} S(t - \Delta t) + \frac{1}{2}\left[e^{-\frac{\Delta t}{\tau_0}} E_x(t - \Delta t) + E_x(t)\right]$$

Let:

$$g = e^{-\frac{\Delta t}{\tau_0}}$$

and denote:

$$\begin{aligned} E_x(x, y, z, t) &\longleftrightarrow E_x^n(i, j, k) \\ S_x(x, y, z, t) &\longleftrightarrow S_x^n(i, j, k) \end{aligned}$$

where the superscript n is the discretized time, and i, j, and k are the discretized x, y, and z coordinates, respectively. Thus:

$$S_x^n(i, j, k) = g S_x^{n-1}(i, j, k) + \frac{1}{2}\left[g E_x^{n-1}(i, j, k) + E_x^n(i, j, k)\right] \tag{2.9}$$

Similar expressions for D_y, S_y and D_z, S_z can be derived using the same technique.

So far, we have examined the Time Domain Maxwell's equations in a Debye medium and derived the expressions for the electric flux density and its first and second derivatives in recursive forms. These expressions will be extensively used in subsequent sections to calculate the electric and magnetic fields.

2.3 Multi-layered Half Space

In this section, we shall study the one-dimensional problem of pulse propagation in Debye media. We shall derive the integro-differential equation in a Debye medium and study the boundary conditions at the interface of two different Debye media. We shall then derive the difference equations for points in the Debye medium and points at the boundary of two different media. We shall also discuss various aspects of the numerical solution including the stability and the simulation of the infinite boundary.

2.3.1 Geometry and Assumptions

We wish to investigate the action of a plane-wave pulse in air with normal incidence on a stratified dispersive medium. The incident pulse can be a ramp signal, electromagnetic pulse (EMP), Gaussian pulse, or others. In the k^{th} layer, the conductivity σ_k is constant and the permittivity $\epsilon_k(t)$ assumes the Debye model. The permittivity for each layer can be written as:

$$\epsilon_k(t) = \epsilon_{k\infty}\delta(t) + \frac{\epsilon_{k0} - \epsilon_{k\infty}}{\tau_{k0}} e^{-\frac{t}{\tau_{k0}}} u(t)$$

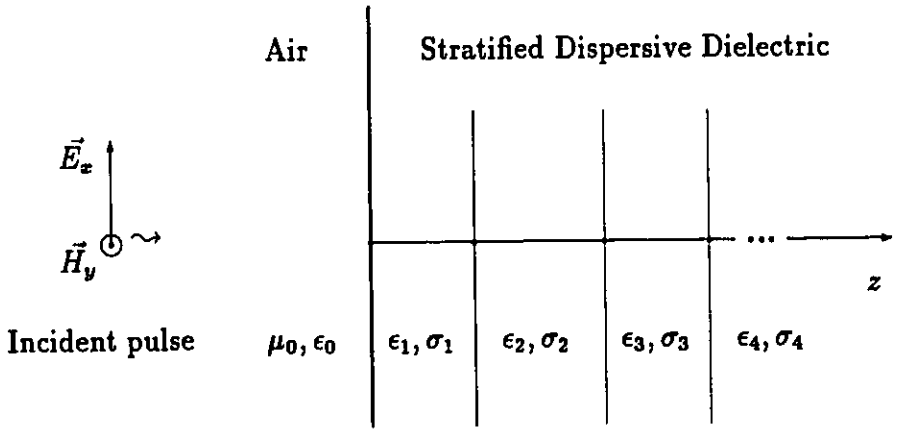

Figure 2.1: Stratified dispersive dielectric irradiated by a plane wave pulse with normal incidence on the air/dielectric interface

2.3.2 Mathematical Formulation

The Differential Equation

Since only E_x and H_y exist for the one-dimensional problem (TEM), then from (2.1) and (2.2), we can write the Maxwell's curl equations in the k^{th} layer as:

$$\begin{aligned} \frac{\partial E_x(z,t)}{\partial z} &= -\mu_0 \frac{\partial H_y(z,t)}{\partial t} \\ -\frac{\partial H_y(z,t)}{\partial z} &= \frac{\partial D_x(z,t)}{\partial t} + \sigma_k E_x(z,t) \end{aligned}$$

or if we combine them and solve for the electric field, as:

$$\frac{\partial^2 D_x(z,t)}{\partial t^2} - \frac{1}{\mu_0}\frac{\partial^2 E_x(z,t)}{\partial z^2} + \sigma_k \frac{\partial E_x(z,t)}{\partial t} = 0. \tag{2.10}$$

Substituting (2.7) into (2.10) and simplifying, we have:

$$\begin{aligned} \frac{\partial^2 E_x(z,t)}{\partial t^2} &= \frac{1}{\mu_0 \epsilon_{k\infty}}\frac{\partial^2 E_x(z,t)}{\partial z^2} - \left(\frac{\sigma_k}{\epsilon_{k\infty}} + \frac{\epsilon_{k0}-\epsilon_{k\infty}}{\epsilon_{k\infty}\tau_{k0}}\right)\frac{\partial E_x(z,t)}{\partial t} \\ &\quad + \frac{\epsilon_{k0}-\epsilon_{k\infty}}{\epsilon_{k\infty}\tau_{k0}^2} E_x(z,t) - \frac{\epsilon_{k0}-\epsilon_{k\infty}}{\epsilon_{k\infty}\tau_{k0}^3}\Delta t S_x(z,t) \end{aligned}$$

Let

$$\begin{aligned} a_k &= \frac{\epsilon_{k0}-\epsilon_{k\infty}}{\epsilon_{k\infty}} \\ \omega_{k0} &= \frac{1}{\tau_{k0}} \\ c_{k\infty} &= \frac{1}{\sqrt{\mu_0 \epsilon_{k\infty}}} \end{aligned}$$

Then

$$\begin{aligned} \frac{\partial^2 E_x(z,t)}{\partial t^2} &= c_{k\infty}^2 \frac{\partial^2 E_x(z,t)}{\partial z^2} - \left(\frac{\sigma_k}{\epsilon_{k\infty}} + a_k\omega_{k0}\right)\frac{\partial E_x(z,t)}{\partial t} \\ &\quad + a_k\omega_{k0}^2 E_x(z,t) - a_k\omega_{k0}^3 \Delta t S_x(z,t) \end{aligned} \tag{2.11}$$

Boundary Conditions

Boundary conditions at the interface are (see Fig. 2.2):

$$E_x(z^-,t) = E_x(z^+,t) \tag{2.12}$$

$$\frac{\partial E_x(z^-,t)}{\partial z} = \frac{\partial E_x(z^+,t)}{\partial z} \tag{2.13}$$

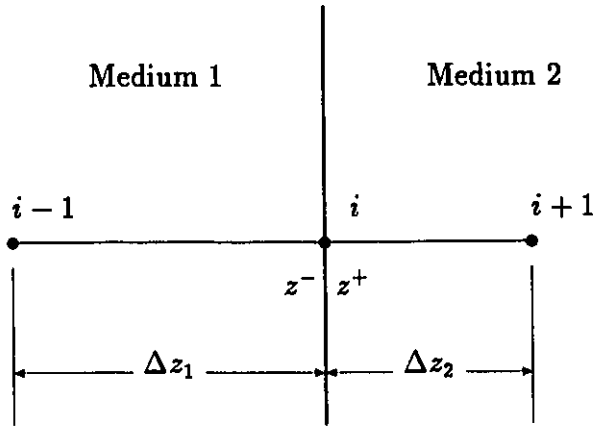

Figure 2.2: Interface between two dispersive media

For medium 1, from (2.11) we have:

$$\frac{\partial^2 E_x(z^-,t)}{\partial t^2} = c_{1\infty}^2 \frac{\partial^2 E_x(z^-,t)}{\partial z^2} - \left(\frac{\sigma_1}{\epsilon_{1\infty}} + a_1\omega_{10}\right)\frac{\partial E_x(z^-,t)}{\partial t} + a_1\omega_{10}^2 E_x(z^-,t) - a_1\omega_{10}^3 \Delta t S_{x1}(z^-,t)\,, \tag{2.14}$$

where

$$S_{x1}(z^-,t) = \frac{1}{\Delta t}\int_0^t e^{-\frac{t-\beta}{\tau_{10}}} E_x(z^-,\beta)d\beta$$

and for medium 2, from equation (2.11) we have:

$$\frac{\partial^2 E_x(z^+,t)}{\partial t^2} = c_{2\infty}^2 \frac{\partial^2 E_x(z^+,t)}{\partial z^2} - \left(\frac{\sigma_2}{\epsilon_{2\infty}} + a_2\omega_{20}\right)\frac{\partial E_x(z^+,t)}{\partial t} + a_2\omega_{20}^2 E_x(z^+,t) - a_2\omega_{20}^3 \Delta t S_{x2}(z^+,t)\,, \tag{2.15}$$

where

$$S_{x2}(z^+,t) = \frac{1}{\Delta t}\int_0^t e^{-\frac{t-\beta}{\tau_{20}}} E_x(z^+,\beta)d\beta$$

By using the Taylor's Series Expansion, we can express E_x as:

$$\begin{aligned} E_x(z^- - \Delta z_1, t) &= E_x(z^-,t) - \Delta z_1 \frac{\partial E_x(z^-,t)}{\partial z} + \frac{\Delta z_1^2}{2}\frac{\partial^2 E_x(z^-,t)}{\partial z^2} \\ E_x(z^+ + \Delta z_2, t) &= E_x(z^+,t) + \Delta z_2 \frac{\partial E_x(z^+,t)}{\partial z} + \frac{\Delta z_2^2}{2}\frac{\partial^2 E_x(z^+,t)}{\partial z^2} \end{aligned}$$

and $\frac{\partial^2 E_x}{\partial z^2}$ as:

$$\begin{aligned} \frac{\partial^2 E_x(z^-,t)}{\partial z^2} &= \frac{2}{\Delta z_1^2}\left[E_x(z^- - \Delta z_1, t) - E_x(z^-,t) + \Delta z_1 \frac{\partial E_x(z^-,t)}{\partial z}\right] \\ \frac{\partial^2 E_x(z^+,t)}{\partial z^2} &= \frac{2}{\Delta z_2^2}\left[E_x(z^+ + \Delta z_2, t) - E_x(z^+,t) - \Delta z_2 \frac{\partial E_x(z^+,t)}{\partial z}\right] \end{aligned}$$

Substituting the above equations into equations (2.14) and (2.15) to eliminate $\frac{\partial^2 E_x}{\partial z^2}$, we subsequently obtain:

$$\begin{aligned} \frac{\partial^2 E_x(z^-,t)}{\partial t^2} &= \frac{2c_{1\infty}^2}{\Delta z_1^2}\left[E_x(z^- - \Delta z_1, t) - E_x(z^-,t) + \Delta z_1 \frac{\partial E_x(z^-,t)}{\partial z}\right] \\ &\quad - \left(\frac{\sigma_1}{\epsilon_{1\infty}} + a_1\omega_{10}\right)\frac{\partial E_x(z^-,t)}{\partial t} \\ &\quad + a_1\omega_{10}^2 E_x(z^-,t) - a_1\omega_{10}^3 \Delta t S_{x1}(z^-,t)\,, \end{aligned} \tag{2.16}$$

and

$$\begin{aligned} \frac{\partial^2 E_x(z^+,t)}{\partial t^2} &= \frac{2c_{2\infty}^2}{\Delta z_2^2}\left[E_x(z^+ + \Delta z_2, t) - E_x(z^+,t) - \Delta z_2 \frac{\partial E_x(z^+,t)}{\partial z}\right] \\ &\quad - \left(\frac{\sigma_2}{\epsilon_{2\infty}} + a_2\omega_{20}\right)\frac{\partial E_x(z^+,t)}{\partial t} \\ &\quad + a_2\omega_{20}^2 E_x(z^+,t) - a_2\omega_{20}^3 \Delta t S_{x2}(z^+,t)\,. \end{aligned} \tag{2.17}$$

Using (2.12) and (2.13) to eliminate $\frac{\partial E}{\partial z}$ in equations (2.16) and (2.17) and simplifying, we obtain:

$$\frac{\partial^2 E_x(z,t)}{\partial t^2} = \left(\frac{c_{1\infty}^2}{\Delta z_1} + \frac{c_{2\infty}^2}{\Delta z_2}\right)^{-1}\left\{\frac{2c_{1\infty}^2 c_{2\infty}^2}{\Delta z_1^2 \Delta z_2}\left[E_x(z^- - \Delta z_1, t) - E_x(z^-,t)\right]\right.$$

$$+\frac{2c_{1\infty}^2c_{2\infty}^2}{\Delta z_1\Delta z_2^2}\left[E_x(z^+ + \Delta z_2, t) - E_x(z^+, t)\right]$$
$$-\left[\frac{c_{2\infty}^2}{\Delta z_2}\left(\frac{\sigma_1}{\epsilon_{1\infty}} + a_1\omega_{10}\right) + \frac{c_{1\infty}^2}{\Delta z_1}\left(\frac{\sigma_2}{\epsilon_{2\infty}} + a_2\omega_{20}\right)\right]\frac{\partial E_x(z,t)}{\partial t}$$
$$+\left(\frac{c_{2\infty}^2}{\Delta z_2}a_1\omega_{10}^2 + \frac{c_{1\infty}^2}{\Delta z_1}a_2\omega_{20}^2\right)E_x(z,t)$$
$$-\frac{c_{2\infty}^2}{\Delta z_2}a_1\omega_{10}^3\Delta t S_{x1}(z^-,t) - \frac{c_{1\infty}^2}{\Delta z_1}a_2\omega_{20}^3\Delta t S_{x2}(z^+,t)\Bigg\}. \quad (2.18)$$

2.3.3 FDTD Implementation

Suppose $f(x)$ is a smooth function of x in an interval $[x_1, x_2]$ and Δx is a small increment of x. Then, the first and second derivatives of $f(x)$ with respect to x can be expressed in the forms of central differences as follows:

$$\frac{\partial f(x)}{\partial x} = \frac{f(x+\Delta x) - f(x-\Delta x)}{2\Delta x}$$

and

$$\frac{\partial^2 f(x)}{\partial x^2} = \frac{f(x+\Delta x) - 2f(x) + f(x-\Delta x)}{\Delta x^2}$$

Equation (2.11) can be rewritten in terms of difference equation as:

$$\frac{E_x^{n+1}(i) - 2E_x^n(i) + E_x^{n-1}(i)}{\Delta t^2} = c_{k\infty}^2\frac{E_x^n(i+1) - 2E_x^n(i) + E_x^n(i-1)}{\Delta z_k^2}$$
$$-\left(\frac{\sigma_k}{\epsilon_{k\infty}} + a_k\omega_{k0}\right)\frac{E_x^{n+1}(i) - E_x^{n-1}(i)}{2\Delta t}$$
$$+ a_k\omega_{k0}^2E_x^n(i) - a_k\omega_{k0}^3\Delta t S_x^n(i)$$

Or as:

$$\alpha E_x^{n+1}(i) = -\beta E_x^{n-1}(i) + \left(\frac{c_{k\infty}\Delta t}{\Delta z_k}\right)^2\left[E_x^n(i+1) - 2E_x^n(i) + E_x^n(i-1)\right]$$
$$+ 2E_x^n(i) + a_k(\omega_{k0}\Delta t)^2E_x^n(i) - a_k(\omega_{k0}\Delta t)^3S_x^n(i)\,, \quad (2.19)$$

where Δt is the time increment, Δz_k is the space increment in the k^{th} layer, and

$$\alpha = 1 + \frac{\Delta t}{2}\left(\frac{\sigma_k}{\epsilon_{k\infty}} + a_k\omega_{k0}\right)$$

$$\beta = 1 - \frac{\Delta t}{2}\left(\frac{\sigma_k}{\epsilon_{k\infty}} + a_k\omega_{k0}\right)$$

and $S_x^n(i)$ computed from (2.9) is:

$$S_x^n(i) = gS_x^{n-1}(i) + \frac{1}{2}\left(gE_x^{n-1}(i) + E_x^n(i)\right).$$

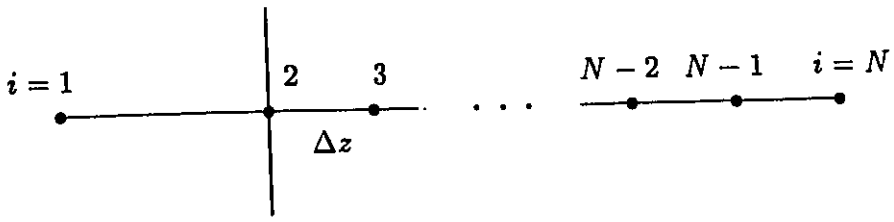

Figure 2.3: Grid points for the FDTD solution. Point $i = 1$ is in air. Point $i = 2$ is at the interface. Point $i = N$ is at the far end.

For the Dielectric/Dielectric Interface, taking the Finite Difference formulation of (2.18) and rearranging, we have:

$$\begin{aligned}
\alpha E_x^{n+1}(i) &= -\beta E_x^{n-1}(i) + \frac{2c_{1\infty}^2 c_{2\infty}^2 \Delta t^2}{\Delta z_1^2 \Delta z_2} E_x^n(i-1) \\
&\quad + \frac{2c_{1\infty}^2 c_{2\infty}^2 \Delta t^2}{\Delta z_1 \Delta z_2^2} E_x^n(i+1) \\
&\quad + \left[\frac{c_{2\infty}^2}{\Delta z_2} a_1(\omega_{10}\Delta t)^2 + \frac{c_{1\infty}^2}{\Delta z_1} a_2(\omega_{20}\Delta t)^2 \right. \\
&\quad \left. + \frac{2c_{1\infty}^2}{\Delta z_1} + \frac{2c_{2\infty}^2}{\Delta z_2} - \frac{2c_{1\infty}^2 c_{2\infty}^2 \Delta t^2}{\Delta z_1 \Delta z_2}\left(\frac{1}{\Delta z_1} + \frac{1}{\Delta z_2}\right)\right] E_x^n(i) \\
&\quad - \frac{c_{2\infty}^2}{\Delta z_2} a_1(\omega_{10}\Delta t)^3 S_{x1}^n(i) \\
&\quad - \frac{c_{1\infty}^2}{\Delta z_1} a_2(\omega_{20}\Delta t)^3 S_{x2}^n(i), \qquad (2.20)
\end{aligned}$$

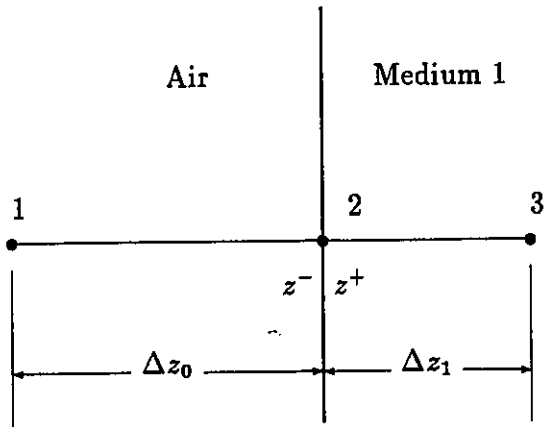

Figure 2.4: Interface between air and dielectric

where

$$\alpha = \frac{c_{1\infty}^2}{\Delta z_1} + \frac{c_{2\infty}^2}{\Delta z_2} + \frac{\Delta t}{2}\left[\frac{c_{2\infty}^2}{\Delta z_2}\left(\frac{\sigma_1}{\epsilon_{1\infty}} + a_1\omega_{10}\right) + \frac{c_{1\infty}^2}{\Delta z_1}\left(\frac{\sigma_2}{\epsilon_{2\infty}} + a_2\omega_{20}\right)\right]$$

$$\beta = \frac{c_{1\infty}^2}{\Delta z_1} + \frac{c_{2\infty}^2}{\Delta z_2} - \frac{\Delta t}{2}\left[\frac{c_{2\infty}^2}{\Delta z_2}\left(\frac{\sigma_1}{\epsilon_{1\infty}} + a_1\omega_{10}\right) + \frac{c_{1\infty}^2}{\Delta z_1}\left(\frac{\sigma_2}{\epsilon_{2\infty}} + a_2\omega_{20}\right)\right].$$

For the Air/Dielectric Interface (see Fig. 2.4):
In equation (2.20), put:

$$\begin{aligned} c_{1\infty} &= c_0 \\ \sigma_1 &= 0 \\ a_1 &= 0 \\ c_{2\infty} &= c_{1\infty} \\ \sigma_2 &= \sigma_1 \\ \epsilon_{2\infty} &= \epsilon_{1\infty} \\ a_2 &= a_1 \\ \omega_{20} &= \omega_{10}\ , \end{aligned}$$

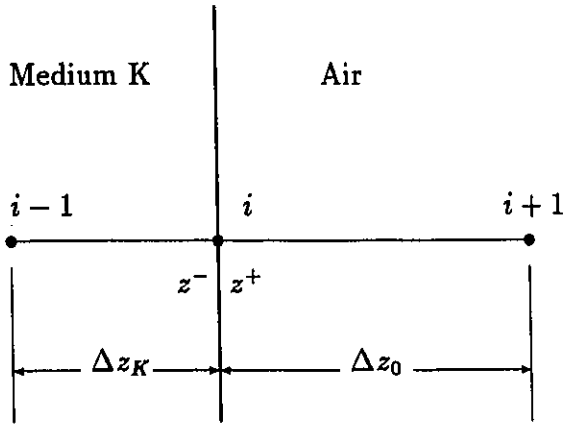

Figure 2.5: Interface between dielectric and air

then

$$\begin{aligned}
\alpha E_x^{n+1}(i) &= -\beta E_x^{n-1}(i) + \frac{2c_0^2 c_{1\infty}^2 \Delta t^2}{\Delta z_0^2 \Delta z_1} E_x^n(i-1) \\
&\quad + \frac{2c_0^2 c_{1\infty}^2 \Delta t^2}{\Delta z_0 \Delta z_1^2} E_x^n(i+1) \\
&\quad + \left[\frac{c_0^2}{\Delta z_0} a_1 (\omega_{10} \Delta t)^2 + \frac{2c_0^2}{\Delta z_0} + \frac{2c_{1\infty}^2}{\Delta z_1} \right. \\
&\quad \left. - \frac{2c_0^2 c_{1\infty}^2 \Delta t^2}{\Delta z_0 \Delta z_1} \left(\frac{1}{\Delta z_0} + \frac{1}{\Delta z_1} \right) \right] E_x^n(i) \\
&\quad - \frac{c_0^2}{\Delta z_0} a_1 (\omega_{10} \Delta t)^3 S_{x1}^n(i) \,, \qquad (2.21)
\end{aligned}$$

where

$$\begin{aligned}
\alpha &= \frac{c_0^2}{\Delta z_0} + \frac{c_{1\infty}^2}{\Delta z_1} + \frac{\Delta t}{2} \frac{c_0^2}{\Delta z_0} \left(\frac{\sigma_1}{\epsilon_{1\infty}} + a_1 \omega_{10} \right) \\
\beta &= \frac{c_0^2}{\Delta z_0} + \frac{c_{1\infty}^2}{\Delta z_1} - \frac{\Delta t}{2} \frac{c_0^2}{\Delta z_0} \left(\frac{\sigma_1}{\epsilon_{1\infty}} + a_1 \omega_{10} \right) .
\end{aligned}$$

For the Dielectric/Air Interface (see Fig. 2.5):

In equation (2.20), put:

$$\begin{aligned} c_{2\infty} &= c_0 \\ \sigma_2 &= 0 \\ a_2 &= 0 \\ c_{1\infty} &= c_{K\infty} \\ \sigma_1 &= \sigma_K \\ \epsilon_{1\infty} &= \epsilon_{K\infty} \\ a_1 &= a_K \\ \omega_{10} &= \omega_{K0}\ , \end{aligned}$$

then

$$\begin{aligned} \alpha E_x^{n+1}(i) &= -\beta E_x^{n-1}(i) + \frac{2c_{K\infty}^2 c_0^2 \Delta t^2}{\Delta z_K^2 \Delta z_0} E_x^n(i-1) \\ &\quad + \frac{2c_{K\infty}^2 c_0^2 \Delta t^2}{\Delta z_K \Delta z_0^2} E_x^n(i+1) \\ &\quad + \left[\frac{c_0^2}{\Delta z_0} a_K (\omega_{K0}\Delta t)^2 + \frac{2c_{K\infty}^2}{\Delta z_K} + \frac{2c_0^2}{\Delta z_0} \right. \\ &\quad \left. - \frac{2c_{K\infty}^2 c_0^2 \Delta t^2}{\Delta z_K \Delta z_0} \left(\frac{1}{\Delta z_K} + \frac{1}{\Delta z_0} \right) \right] E_x^n(i) \\ &\quad - \frac{c_0^2}{\Delta z_0} a_K (\omega_{K0}\Delta t)^3 S_{xK}^n(i)\ , \end{aligned} \tag{2.22}$$

where

$$\begin{aligned} \alpha &= \frac{c_{K\infty}^2}{\Delta z_K} + \frac{c_0^2}{\Delta z_0} + \frac{\Delta t}{2} \frac{c_0^2}{\Delta z_0} \left(\frac{\sigma_K}{\epsilon_{K\infty}} + a_K \omega_{K0} \right) \\ \beta &= \frac{c_{K\infty}^2}{\Delta z_K} + \frac{c_0^2}{\Delta z_0} - \frac{\Delta t}{2} \frac{c_0^2}{\Delta z_0} \left(\frac{\sigma_K}{\epsilon_{K\infty}} + a_K \omega_{K0} \right). \end{aligned}$$

2.3.4 Practical Aspects of a Difference solution

Stability Criterion

For stability, the following condition must be satisfied (see Appendix B for details):

$$\Delta z \leq c_\infty \Delta t$$

Choosing:

$$\Delta z = c_\infty \Delta t$$

results in three advantages [16]:

- The time increment Δt is the largest one permitted, thus allowing a problem to be solved with the minimal number of time steps.
- The calculations at each step are reduced to a minimum because equation (2.19) simplifies greatly.
- The exact solution is obtained because the truncation error in (2.19) vanishes.

Simulation of Infinite Boundary

For the far-end boundary, the infinite boundary can be terminated at the point [16]:

$$I_{END} \geq I_{obs} + \frac{N - I_{obs}}{2} + 1 \,,$$

where

$$\begin{aligned} I_{END} &= \text{truncation point} \\ I_{obs} &= \text{observation point} \\ N &= \text{number of time step to be calculated.} \end{aligned}$$

When the above condition is satisfied, the back scattered signal originating at the truncation point does not reach the observation point.

2.3.5 Description of the Computer Program

A one-dimensional FDTD program has been developed based on the theory presented in this section. The program has been written specifically for a stratified half space filled with Debye media. The incident field in air impinges normally on the air-dielectric interface. A FORTRAN listing of the program may be found in Appendix C.

The program may be divided into two major sections: the data input section, and the iteration section. The data input section is the part of the program which prompts the user for the data necessary to define the problem, and it also calculates the necessary coefficients to be used in the iteration section. The iteration section is the part of the program which calculates the electric fields at every point of the mesh based on the information obtained in the data input section, and on the electric fields at previous time steps. The iteration continues until a solution is obtained for every time step inside the desired time window.

The program outputs are either the electric field distribution at specific times, or the electric field as a function of time at specific points in space.

In this section, we have derived the integro-differential equations for the propagation in a Debye medium (2.11) and at the boundary of two different Debye media (2.18). We have also presented these equations in explicit difference forms (2.19), (2.20), (2.21), and (2.22). These equations were used in the computer program which calculated the transmitted fields in stratified Debye half space (Appendix C). The stability criterion and the simulation of infinite boundary developed above were also used in the program to ensure the stable and accurate solution.

2.4 Multi-layered Circular Cylinder

In this section, we shall examine the Time Domain Maxwell's equations in a Debye medium applied to two-dimensional problems. We shall also study the boundary conditions at the interface of two different Debye media. The explicit difference equations for points in a Debye medium will be derived. The stability and the absorbing boundary conditions will also be studied in detail.

2.4.1 Geometry and Assumptions

The geometry under consideration (see Fig. 2.6) consists of an infinitely long multilayered circular cylinder of dispersive dielectric in free space. We consider a transient electromagnetic plane-wave incident from free space on the cylinder.

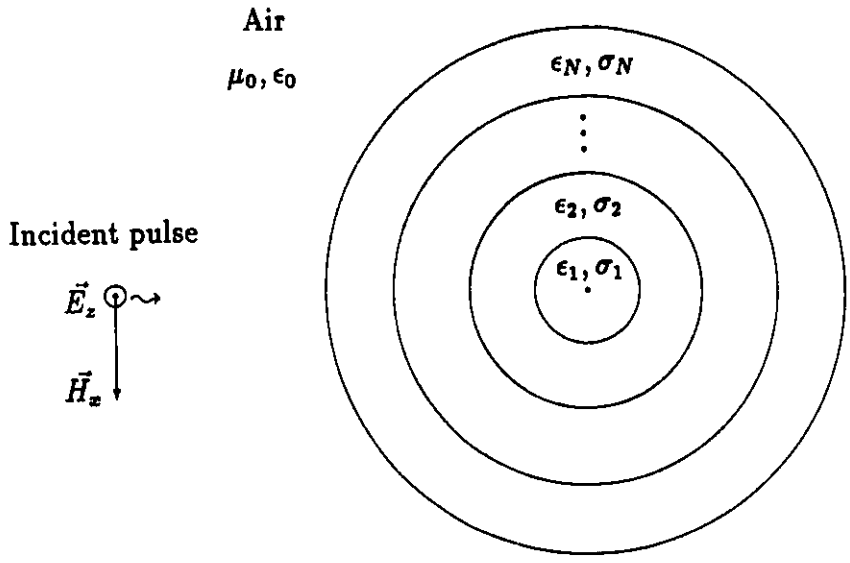

Figure 2.6: Multi-layered circular cylinder exposed to a plane wave pulse. E-field is parallel to the axis of the cylinder.

We distinguish two cases: The case in which the incident electric field

is parallel to the axis of the cylinder and the case in which the incident magnetic field is parallel to the axis of cylinder, with the general case is a linear combination of the two. In this section, we shall investigate only the former case. The solution for the later case can be easily derived using the same technique. As in the previous section, the dielectric in each layer is assumed to be of the Debye model.

2.4.2 Mathematical Formulation

The Differential Equations

For the case in which the electric field is parallel to the z-axis, only E_z, H_x, and H_y exist. From Maxwell's equations (2.1) and (2.2), we have:

$$\frac{\partial E_z(x,y,t)}{\partial y} = -\mu_0 \frac{\partial H_x(x,y,t)}{\partial t} \tag{2.23}$$

$$\frac{\partial E_z(x,y,t)}{\partial x} = \mu_0 \frac{\partial H_y(x,y,t)}{\partial t} \tag{2.24}$$

$$\frac{\partial H_y(x,y,t)}{\partial x} - \frac{\partial H_x(x,y,t)}{\partial y} = \frac{\partial D_z(x,,y,t)}{\partial t} + \sigma_k E_z(x,y,t) \tag{2.25}$$

Substituting (2.6) into (2.25) results in:

$$\begin{aligned}
\frac{\partial H_x(x,y,t)}{\partial t} &= -\frac{1}{\mu_0}\frac{\partial E_z(x,y,t)}{\partial y} \\
\frac{\partial H_y(x,y,t)}{\partial t} &= \frac{1}{\mu_0}\frac{\partial E_z(x,y,t)}{\partial x} \\
\frac{\partial E_z(x,y,t)}{\partial t} &= \frac{1}{\epsilon_{k\infty}}\left[\frac{\partial H_y(x,y,t)}{\partial x} - \frac{\partial H_x(x,y,t)}{\partial y}\right. \\
&\quad \left. - \left(\sigma_k + \frac{\epsilon_{k0}-\epsilon_{k\infty}}{\tau_{k0}}\right) E_z(x,y,t) + \frac{\epsilon_{k0}-\epsilon_{k\infty}}{\tau_{k0}^2}\Delta t S_z(x,y,t)\right]
\end{aligned}$$

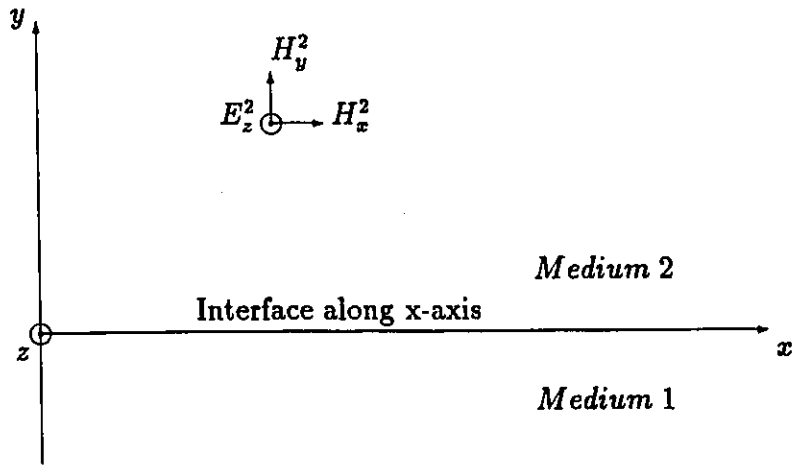

Figure 2.7: Continuity at the interface along x-axis. E-field is in the z direction. The wave propagates in the $+y$ direction.

Boundary Conditions

Consider the plane interface along x-axis separating medium 1 and medium 2 (see Fig. 2.7).

The continuity condition at the interface imposes the following conditions [20]:

$$\begin{aligned} E_z^1 &= E_z^2 \\ \frac{\partial E_z^1}{\partial x} &= \frac{\partial E_z^2}{\partial x} \\ H_y^1 &= H_y^2 \\ \frac{\partial H_y^1}{\partial x} &= \frac{\partial H_y^2}{\partial x} \\ H_x^1 &= H_x^2 \end{aligned}$$

From (2.23), we have:

$$\frac{\partial E_z^1}{\partial y} = \frac{\partial E_z^2}{\partial y}$$

Therefore, both E_z and $\frac{\partial E_z}{\partial y}$ are continuous across the interface.
From (2.25), we have:

$$\frac{\partial H_x^1}{\partial y} - \frac{\partial H_x^2}{\partial y} = \frac{\partial D_z^2}{\partial t} - \frac{\partial D_z^1}{\partial t} + (\sigma_2 - \sigma_1)E_z \tag{2.26}$$

This equation indicates that $\frac{\partial H_x}{\partial y}$ has a finite discontinuity across the interface. Thus, if we choose the grid points such that H_x 's are on the interface, the boundary conditions at the interface will be automatically satisfied.

2.4.3 FDTD Implementation

If we substitute central differences for the derivatives of E and H in equations (2.23),(2.24), and (2.25), and if we denote:

$$E_z^n(i,j) \longleftrightarrow E_z(x,y,t)\,,$$

then we obtain:

$$\begin{aligned}
\frac{H_x^{n+\frac{1}{2}}(i,j+\frac{1}{2}) - H_x^{n-\frac{1}{2}}(i,j+\frac{1}{2})}{\Delta t} &= -\frac{1}{\mu_0}\frac{E_z^n(i,j+1) - E_z^n(i,j)}{\Delta y} \\
\frac{H_y^{n+\frac{1}{2}}(i+\frac{1}{2},j) - H_y^{n-\frac{1}{2}}(i+\frac{1}{2},j)}{\Delta t} &= -\frac{1}{\mu_0}\frac{E_z^n(i+1,j) - E_z^n(i,j)}{\Delta x} \\
\frac{E_z^{n+1}(i,j) - E_z^n(i,j)}{\Delta t} &= \frac{1}{\epsilon_{k\infty}}\Bigg[-\left(\sigma_k + \frac{\epsilon_{k0} - \epsilon_{k\infty}}{\tau_{k0}}\right)E_z^n(i,j) \\
&\quad + \frac{H_y^{n+\frac{1}{2}}(i+\frac{1}{2},j) - H_y^{n+\frac{1}{2}}(i-\frac{1}{2},j)}{\Delta x} \\
&\quad - \frac{H_x^{n+\frac{1}{2}}(i,j+\frac{1}{2}) - H_x^{n+\frac{1}{2}}(i,j-\frac{1}{2})}{\Delta y} \\
&\quad + \frac{\epsilon_{k0} - \epsilon_{k\infty}}{\tau_{k0}^2}\Delta t S_z^n(i,j)\Bigg]
\end{aligned}$$

Note that E is defined on the mesh nodes but that H is defined between these nodes. And, E and H are evaluated at alternate half-time steps.
We choose

$$\Delta x = \Delta y = \Delta l\,,$$

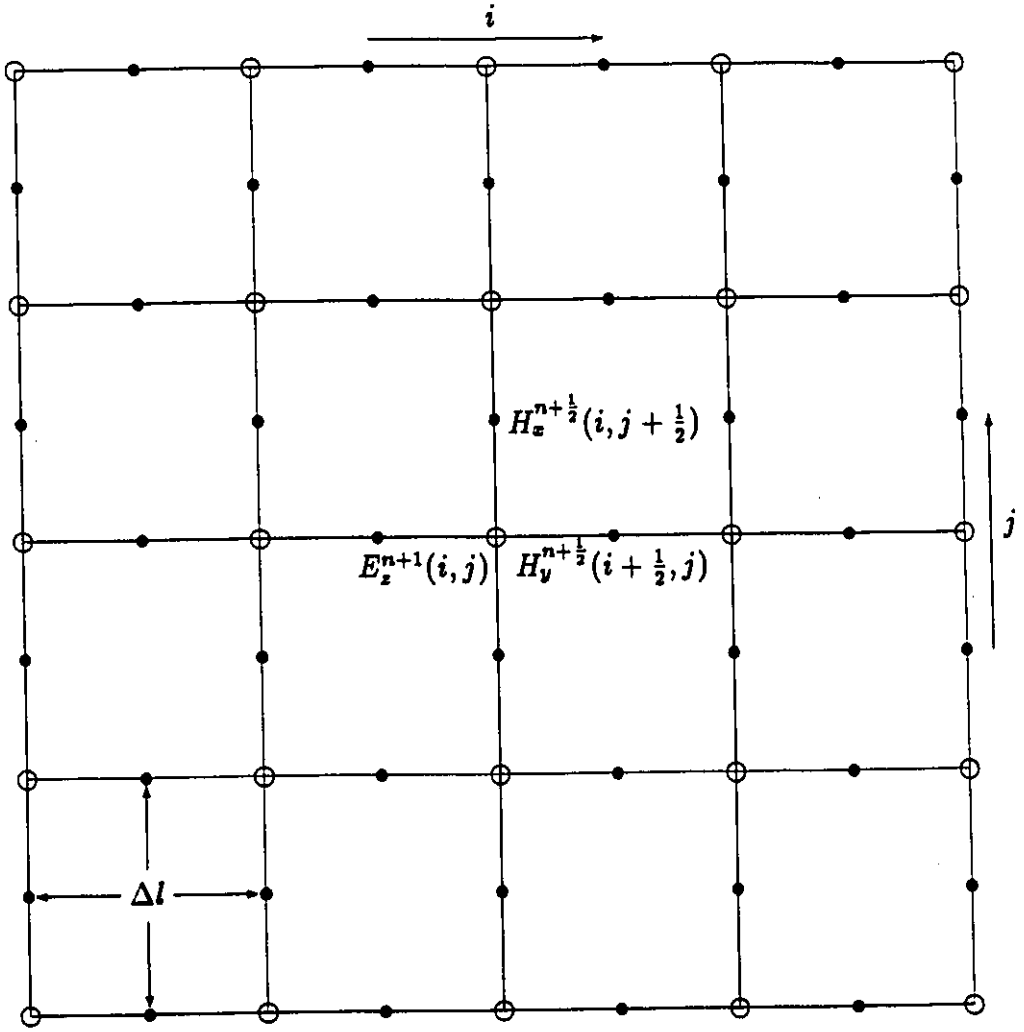

Figure 2.8: The mesh for two dimensional FDTD.

thus creating a grid mesh of equally spaced nodes (see Fig. 2.8). The magnetic field H and the electric field E are described using finite differences as:

$$H_x^{n+\frac{1}{2}}(i,j+\frac{1}{2}) = H_x^{n-\frac{1}{2}}(i,j+\frac{1}{2}) - \frac{\Delta t}{\mu_0 \Delta l}\left[E_z^n(i,j+1) - E_z^n(i,j)\right] , \quad (2.27)$$

$$H_y^{n+\frac{1}{2}}(i+\frac{1}{2},j) = H_y^{n-\frac{1}{2}}(i+\frac{1}{2},j) + \frac{\Delta t}{\mu_0 \Delta l}\left[E_z^n(i+1,j) - E_z^n(i,j)\right] , \quad (2.28)$$

$$\begin{aligned} E_z^{n+1}(i,j) = {} & \left[1 - \Delta t\left(\frac{\sigma_k}{\epsilon_{k\infty}} + \frac{\epsilon_{k0}-\epsilon_{k\infty}}{\epsilon_{k\infty}\tau_{k0}}\right)\right] E_z^n(i,j) \\ & + \frac{\Delta t}{\epsilon_{k\infty}\Delta l}\left\{H_y^{n+\frac{1}{2}}(i+\frac{1}{2},j) - H_y^{n+\frac{1}{2}}(i-\frac{1}{2},j) \right. \\ & \left. - \left[H_x^{n+\frac{1}{2}}(i,j+\frac{1}{2}) - H_x^{n+\frac{1}{2}}(i,j-\frac{1}{2})\right]\right\} \\ & + \left(\frac{\epsilon_{k0}-\epsilon_{k\infty}}{\epsilon_{k\infty}}\right)(\omega_{k0}\Delta t)^2 S_z^n(i,j) , \end{aligned} \quad (2.29)$$

where

$$S_z^n(i,j) = gS_z^{n-1}(i,j) + \frac{1}{2}\left(gE_z^{n-1}(i,j) + E_z^n(i,j)\right) .$$

2.4.4 Practical Aspects of a Difference Solution

Stability Criterion

For any given cell size Δl, there is a restriction on the step Δt to ensure stability. This restriction can be described as [21]:

$$v_{max}\Delta t \leq \left(\frac{1}{\Delta x^2} + \frac{1}{\Delta y^2}\right)^{-\frac{1}{2}} ,$$

where v_{max} is the velocity of the propagating wave. Since the cylinder is in free space:

$$v_{max} = c_0 ,$$

where c_0 is the velocity of light in free space, and

$$\Delta x = \Delta y = \Delta l \, .$$

Thus the stability criterion can be written as:

$$c_0 \Delta t \leq \frac{\Delta l}{\sqrt{2}} \, ,$$

or as:

$$\frac{\Delta t}{\Delta l} \leq \frac{1}{c_0 \sqrt{2}} \, .$$

Absorbing Boundary Conditions

The problem is an open problem, but because the domain in which we compute the field is limited, we must create absorbing boundary conditions at the artificial boundaries produced by truncating the mesh to simulate the conditions of unbounded space. For finite difference approximations of Maxwell's equations, absorbing boundary conditions have been described by a number of authors [27], [21], [23], [24], [25], [26]. The absorbing conditions used here are those suggested by Reynolds [26].
Suppose the wave equation is given by:

$$\frac{1}{c_0^2} \frac{\partial^2 u}{\partial t^2} = \frac{\partial^2 u}{\partial x^2} + \frac{\partial^2 u}{\partial y^2}$$

where c_0 is the velocity of light in free space.
and suppose the domain is truncated at $x = -a$, $x = a$, $y = -b$, and $y = b$, then the absorbing boundary conditions are:

$$\left(\frac{1}{c_0} \frac{\partial}{\partial t} - \frac{\partial}{\partial x} \right) \left(\frac{p}{c_0} \frac{\partial}{\partial t} - \frac{\partial}{\partial x} \right) u = 0 \, , \; x = -a$$

$$\left(\frac{1}{c_0} \frac{\partial}{\partial t} + \frac{\partial}{\partial x} \right) \left(\frac{p}{c_0} \frac{\partial}{\partial t} + \frac{\partial}{\partial x} \right) u = 0 \, , \; x = a$$

$$\left(\frac{1}{c_0} \frac{\partial}{\partial t} - \frac{\partial}{\partial y} \right) \left(\frac{p}{c_0} \frac{\partial}{\partial t} - \frac{\partial}{\partial y} \right) u = 0 \, , \; y = -b$$

$$\left(\frac{1}{c_0}\frac{\partial}{\partial t}+\frac{\partial}{\partial y}\right)\left(\frac{p}{c_0}\frac{\partial}{\partial t}+\frac{\partial}{\partial y}\right)u=0\ ,\ y=b$$

where

$$p=\frac{c_0\Delta t}{\Delta l}$$

Apply the absorbing boundary conditions for FDTD with the mesh size (I_{max}, J_{max}), we have:

For boundary $i=1$:

$$u_{1,j}^{n+1}=u_{1,j}^{n}+u_{2,j}^{n}-u_{2,j}^{n-1}+p\left[u_{2,j}^{n}-u_{1,j}^{n}-\left(u_{3,j}^{n-1}-u_{2,j}^{n-1}\right)\right]$$

For boundary $i=I_{max}+1$:

$$\begin{aligned}u_{I_{max}+1,j}^{n+1} &= u_{I_{max}+1,j}^{n}+u_{I_{max},j}^{n}-u_{I_{max},j}^{n-1}\\ &\quad +p\left[u_{I_{max},j}^{n}-u_{I_{max}+1,j}^{n}\left(u_{I_{max}-1,j}^{n-1}-u_{I_{max},j}^{n-1}\right)\right]\end{aligned}$$

For boundary $j=1$:

$$u_{i,1}^{n+1}=u_{i,1}^{n}+u_{i,2}^{n}-u_{i,2}^{n-1}+p\left[u_{i,2}^{n}-u_{i,1}^{n}-\left(u_{i,3}^{n-1}-u_{i,2}^{n-1}\right)\right]$$

For boundary $j=J_{max}+1$:

$$\begin{aligned}u_{i,J_{max}+1}^{n+1} &= u_{i,J_{max}+1}^{n}+u_{i,J_{max}}^{n}-u_{i,J_{max}}^{n-1}\\ &\quad +p\left[u_{i,J_{max}}^{n}-u_{i,J_{max}+1}^{n}\left(u_{i,J_{max}-1}^{n-1}-u_{i,J_{max}}^{n-1}\right)\right]\end{aligned}$$

Special boundary conditions for the corners of the mesh are:

$$\begin{aligned}u_{1,1}^{n+1} &= u_{1,1}^{n}+p\left(u_{2,2}^{n}-u_{1,1}^{n}\right)\\ u_{I_{max}+1,1}^{n+1} &= u_{I_{max}+1,1}^{n}+p\left(u_{I_{max},2}^{n}-u_{I_{max}+1,1}^{n}\right)\\ u_{1,J_{max}+1}^{n+1} &= u_{1,J_{max}+1}^{n}+p\left(u_{2,J_{max}}^{n}-u_{1,J_{max}+1}^{n}\right)\\ u_{I_{max}+1,J_{max}+1}^{n+1} &= u_{I_{max}+1,J_{max}+1}^{n}+p\left(u_{I_{max},J_{max}}^{n}-u_{I_{max}+1,J_{max}+1}^{n}\right)\end{aligned}$$

In summary, the entire domain of computation can be divided into two subdomains: a subdomain for the FDTD computation and a subdomain for the absorbing boundary (see Fig. 2.9). In the subdomain for the FDTD computation, the equations derived in section 2.4.3 are used. However, in the subdomain for the absorbing boundary, the equations presented in section 2.4.4 must be used. A final remark is that the absorbing boundary conditions are correct only for outgoing waves. Thus, to use the absorbing boundary conditions, we must eliminate the incident field by subtracting it from the total field.

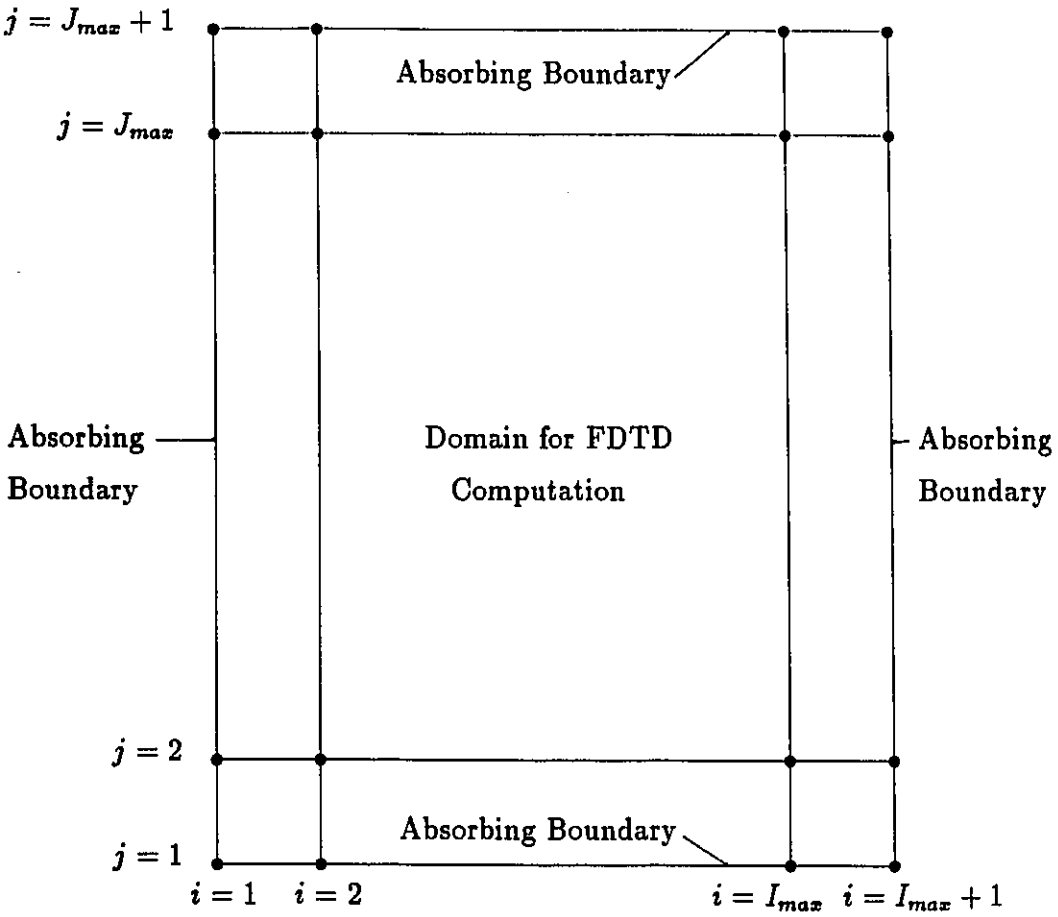

Figure 2.9: Domain for FDTD and the absorbing boundaries: $i = 1$, $i = I_{max} + 1$, $j = 1$, and $j = J_{max} + 1$.

2.4.5 Description of the Computer Program

A two-dimensional FDTD program has been developed based on the theory presented in this section. The program has been written specifically for a multilayereded circular cylinder filled with Debye media. The cylinder was assumed to be infinite in the z direction. The incident wave was assumed to be a $+y$ directed plane wave whose electric field vector is in the z direction. A FORTRAN listing of the program for a continuous incident wave may be found in Appendix E and a FORTRAN listing of the program for a pulsed incident wave may be found in Appendix F.

The program consists of two major sections: the data input section and the iteration section. The data input section is the part of the program which prompts the user for the data necessary to define the problem and then calculates the necessary coefficients to be used in the iteration section. The iteration section is the part of the program which calculates the electric fields at every point of the mesh based on the information obtained in the data input section and on the electric fields at previous time steps. The iteration continues until a solution is obtained for every time step inside the desired time window.

The program outputs are the electric field distributions along the diameter parallel to the y-axis at specific times.

In this section, we have studied the Time Domain Maxwell's equations in a Debye medium applied to a two-dimensional problem and the boundary conditions at the interface of two different Debye media. We have derived the explicit difference equations for E_z, H_x, and H_y for the case in which the electric field is parallel to the z direction. We have proved, for this case, that if we choose the grid points at the interface of two different media properly, the boundary conditions at the interface will be automatically satisfied. We have also studied the stability and the absorbing boundary conditions to ensure a stable and accurate solution.

Chapter 3

Numerical Results

3.1 Introduction

This chapter presents the numerical results of the FDTD method applied to various dielectric structures and for different types of incident pulses.

Four cases of the one-dimensional problem were investigated. First, the reflected fields at the interface of a homogeneous half space filled with a Debye dielectric were calculated. The incident field was a time dependent ramp function with various rise-times. Second, the transmitted waveforms inside a homogeneous half space filled with muscle were computed at different depths. The incident fields were EMP and Gaussian pulses. The third case was similar to the second case except that the muscle was replaced by fat and the incident field was an EMP pulse. Finally, the transmitted fields inside a stratified half space filled with skin, fat, and muscle were calculated. The incident field was an EMP pulse.

For the two-dimensional problem, the above four cases, with some changes in geometry, were also studied. The changes were the substitutions of the homogeneous half space by a homogeneous circular cylinder and the stratified half space by a multilayered circular cylinder.

3.2 One-dimensional Problems

In this section, the geometry of the media was assumed to be in the form of an infinite half space. The incident field irradiated normally from the air on

the air-dielectric interface.

3.2.1 Homogeneous Half Space of Debye Medium

For comparison, the data used in this case were those used by Bolomey *et al* [17]. The medium was assumed to have a conductivity $\sigma = 0$, a low frequency permittivity $\epsilon_0 = 13$, a high frequency permittivity $\epsilon_\infty = 2$, and an angular relaxation frequency $\omega_0 = 10^9\ rad/$. The incident field was a ramp function with various rise times $t_r = 1.5\ ns$, $0.1\ ns$, $0.02\ ns$, $8\ ps$, $2\ ps$, and $0.001\ ps$. Δt was chosen to be equal to the rise time divided by 200. The reflected fields at the air-dielectric interface were calculated for each rise time. The program was time stepped to 800 time steps.

Figure 3.4 shows the reflected fields at the air-dielectric interface for various rise times.

3.2.2 Homogeneous Half Space of Muscle

For comparison with the results obtained by Lin [11], the medium which was investigated was muscle. According to Lin, muscle has a conductivity $\sigma = 0$, a low frequency permittivity $\epsilon_0 = 2.55 \times 10^6$, a high frequency permittivity $\epsilon_\infty = 0.2 \times 10^6$, and an angular relaxation frequency $\omega_0 = 502.65\ rad/s$.

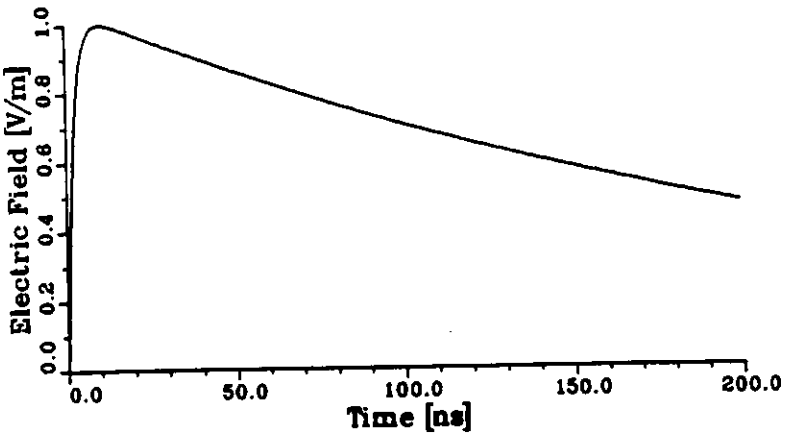

Figure 3.1: Incident EMP in air at z = 0 as a function of time.

Figure 3.5 shows the transmitted fields at various depths $z = 0$, 1, 2, and 3 cm for an EMP incident field characterized by [37]:

$$E_0(t) = 1.05016 \times \left(e^{-4.0\times10^6 t} - e^{-4.76\times10^8 t}\right) \ (V/m)$$

The peak amplitude of the pulse is 1 V/m at $t = 10$ ns (see Fig. 3.1). The Δt was chosen to be equal to 0.1 ns. The program was time stepped to 2000 time steps.

Figures 3.6 and 3.7 show the transmitted fields at various depths $z = 0$, 10, 20, and 30 cm for Gaussian incident pulses with $t_1 = 1$ μs and $t_1 = 50$ μs, respectively. The Δt was chosen to be equal to 0.01 μs and 1 μs, respectively. The program was time stepped to 1400 and 700 time steps, respectively. A Gaussian pulse is given by [11]:

$$E_0(z,t) = e^{-\frac{\left(t-\frac{z}{c_0}\right)^2}{2t_1^2}}$$

where t_1 is the pulse width in time, c_0 is the velocity of light in free space, and $z = 0$ at the interface (see Fig. 3.2).

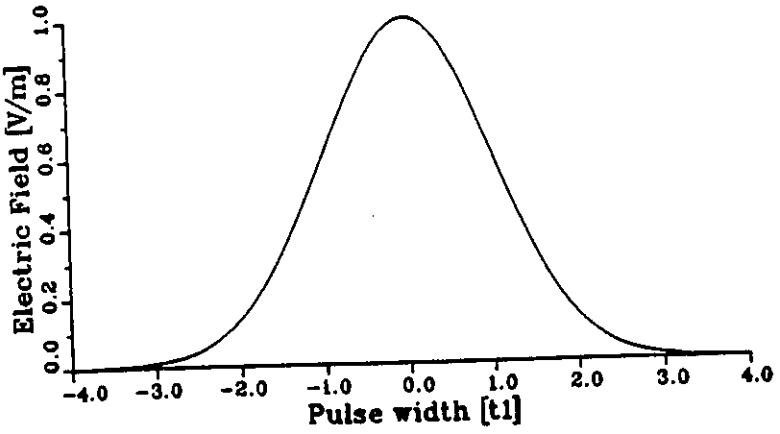

Figure 3.2: Incident Gaussian Pulse in air at z = 0 as a function of time.

3.2.3 Homogeneous Half Space of Fat

The medium which was investigated was fat which has a conductivity $\sigma = 0$, a low frequency permittivity $\epsilon_0 = 46.9$, a high frequency permittivity $\epsilon_\infty = 5.51$, and an angular relaxation frequency $\omega_0 = 5.55 \times 10^8\ rad/s$. These parameters were obtained by converting the data collected by Stuchly [32] into the Cole-Cole form using the least-square method. The Δt was chosen to be equal to 0.1 ns. The program was time stepped to 1000 time steps.

Figure 3.8 shows the transmitted field at the air dielectric interface for an EMP incidence. The half space is filled with fat, with dielectric constant of $\epsilon_r = \epsilon_0$, or with dielectric constant of $\epsilon_r = \epsilon_\infty$.

Figure 3.9 is the same as Fig. 3.8 but at a larger scale.

3.2.4 Stratified Half Space of Skin, Fat and Muscle

Skin layer with a thickness of 1 mm has a conductivity $\sigma = 0$, a low frequency permittivity $\epsilon_0 = 700$, a high frequency permittivity $\epsilon_\infty = 41.7$, and an angular relaxation frequency $\omega_0 = 6.67 \times 10^8\ rad/s$. Fat layer with a thickness of 5 mm has a conductivity $\sigma = 0$, a low frequency permittivity $\epsilon_0 = 46.9$, a high frequency permittivity $\epsilon_\infty = 5.51$, and an angular relaxation frequency $\omega_0 = 5.55 \times 10^8\ rad/s$. Muscle layer with infinite thickness has a conductivity $\sigma = 0$, a low frequency permittivity $\epsilon_0 = 6.15 \times 10^5$, a high frequency permittivity $\epsilon_\infty = 1.032 \times 10^3$, and an angular relaxation frequency $\omega_0 = 22.353 \times 10^3\ rad/s$. The parameters of skin, fat, and muscle were obtained by converting the data collected by Stuchly [32] into the Cole-Cole form using the least-square method. The Δt was chosen to be equal to 10 ps. The program was time stepped to 10,000 time steps.

Figure 3.10 shows the transmitted field as a function of time at various depths $z = 0$, 1, 6, 10, and 20 mm.

Figure 3.11 shows the electric field distributions in space at various times $t = 0.1$, 0.2, 1, 5, and 10 ns.

Figures 3.12 and 3.13 are the same as Fig. 3.10 but at larger scales to observe multiple reflections.

3.3 Two-dimensional Problems

In this section, the geometry of the media was assumed to be in the form of a circular cylinder infinitely long in the z direction. The incident wave was assumed to be a $+y$-directed plane wave whose electric field vector is in the z direction. Because there is no variation of either scatterer geometry or incident fields in the z direction, this problem is treated as the two-dimensional scattering of the incident wave, with only E_z, H_x, and H_y fields present.

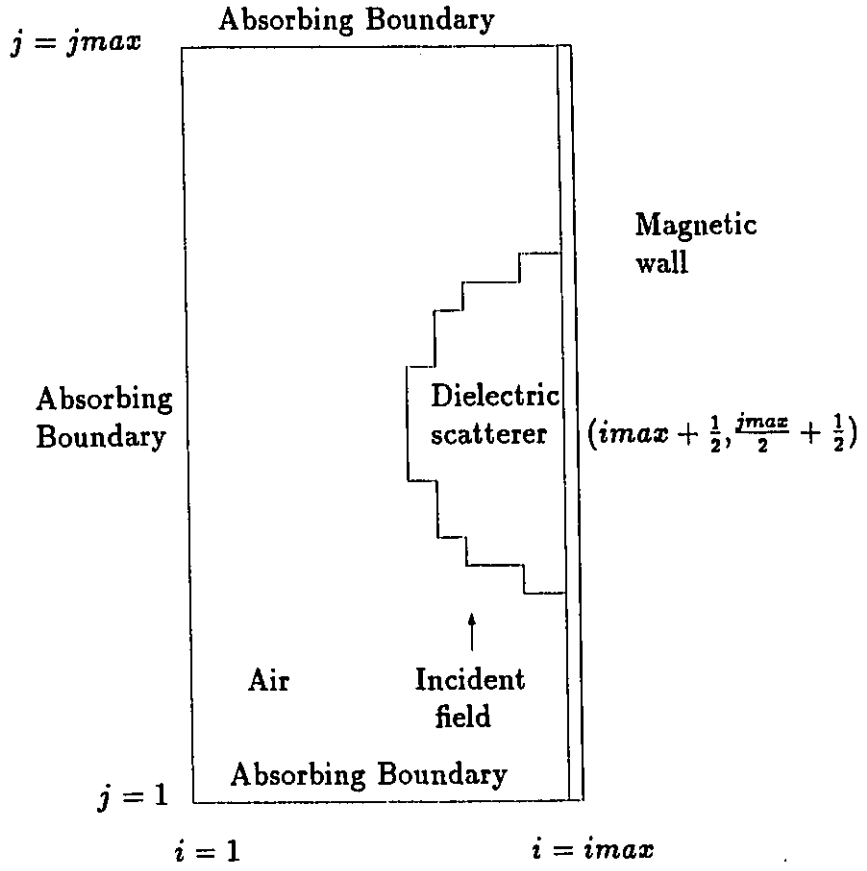

Figure 3.3: Geometry of the scatterer relative to the grid.

The two-dimensional grid was used. The geometry of the scatterer relative

to the grid is illustrated in Fig. 3.3. The cylinder axis was chosen as the line $(imax\frac{1}{2}, (\frac{jmax}{2})\frac{1}{2}, k)$. Because the scatterer was evenly symmetric about the grid line $i = imax\frac{1}{2}$, we had the symmetry condition:

$$E_z^n(imax + 1, j) = E_z^n(imax, j)$$

Absorbing boundary conditions were used to truncate the grid at $i = 1$, $j = 1$, and $j = jmax$.

3.3.1 Homogeneous Circular Dielectric Cylinder

For comparison, the data used for calculations in this case were those used by Taflove *et al* [21]. The dielectric had a conductivity $\sigma = 0$, a relative permittivity $\epsilon_r = 4$. The incident field was a continuous, sinusoidal plane wave of frequency $f = 2.5\ GHz$. The diameter of the cylinder was one wavelength in free space (12 cm).

The geometry of the cylinder relative to the grid was the same as that illustrated in Fig. 3.3 with $imax = 25$, $jmax = 50$. The cylinder axis was chosen as the line $(25\frac{1}{2}, 25\frac{1}{2}, k)$. Because the scatterer was evenly symmetric about the grid line $i = 25\frac{1}{2}$, the symmetry condition was:

$$E_z^n(26, j) = E_z^n(25, j)$$

Absorbing boundary conditions were used to truncate the grid at $i = 1$, $j = 1$, and $j = 50$.The incident wave was generated at line $j = 3$.
The grid coordinates inside the cylinder were determined by:

$$((i - 25\frac{1}{2})^2 + (j - 25\frac{1}{2})^2)^{\frac{1}{2}} \leq 20$$

The node separation was chosen to be $\Delta l = 0.3\ cm$ and the time increment $\Delta t = 5\ ps$. The program was time stepped to 500 time steps.

The envelope of E_z for $460 \leq n \leq 500$ is plotted in Fig. 3.14 with the analytical solution calculated using the summed-series technique [10] for comparison (see Appendix D). In Fig. 3.14, the radius of the cylinder was normalized to 1.

3.3.2 Homogeneous Circular Cylinder of Muscle

The medium which was investigated was muscle which has a conductivity $\sigma = 0$, a low frequency permitivity $\epsilon_0 = 6.15 \times 10^5$, a high frequency permitivity $\epsilon_\infty = 1.032 \times 10^3$, and an angular relaxation frequency $\omega_0 = 22.353 \times 10^3\ rad/s$. The radius of the cylinder was 12 cm. The incident field was a Gaussian pulse with $t_1 = 1\ ns$.

The geometry of the cylinder relative to the grid was the same as that illustrated in Fig. 3.3 with $imax = 25$, $jmax = 50$. The cylinder axis was chosen as the line $(25\frac{1}{2}, 25\frac{1}{2}, k)$. Because the scatterer was evenly symmetric about the grid line $i = 25\frac{1}{2}$, the symmetry condition was:

$$E_z^n(26, j) = E_z^n(25, j)$$

Absorbing boundary conditions were used to truncate the grid at $i = 1$, $j = 1$, and $j = 50$.The incident wave was generated at line $j = 3$.

The node separation was chosen to be $\Delta l = 0.6\ cm$ and the time increment $\Delta t = 10\ ps$. Then, the radius length was subdivided into 20 segments. Thus, the grid coordinates inside the cylinder were determined by:

$$((i - 25\frac{1}{2})^2 + (j - 25\frac{1}{2})^2)^{\frac{1}{2}} \leq 20$$

The program was initialized at $t = -4t_1$ $(-4\ ns)$ and time stepped to 6 ns (1000 time steps).

Figure 3.15 shows the electric field distributions along the diameter parallel to the propagation direction of the incident pulse at various times $t = 1$, 3, and 6 ns. In Fig. 3.15, the radius of the cylinder was normalized to 1.

3.3.3 Homogeneous Circular Cylinder of Fat

The parameters of the medium were those used in section 3.2.3. The radius of the cylinder was 12 cm. The incident field was either an EMP or a Gaussian pulse of pulse width of 0.2 ns.

The geometry of the cylinder relative to the grid was the same as that illustrated in Fig. 3.3 with $imax = 25$, $jmax = 50$. The cylinder axis was chosen as the line $(25\frac{1}{2}, 25\frac{1}{2}, k)$. Because the scatterer was evenly symmetric about the grid line $i = 25\frac{1}{2}$, the symmetry condition was:

$$E_z^n(26, j) = E_z^n(25, j)$$

Absorbing boundary conditions were used to truncate the grid at $i = 1$, $j = 1$, and $j = 50$. The incident wave was generated at line $j = 3$.

The node separation was chosen to be $\Delta l = 0.6\ cm$ and the time increment $\Delta t = 10\ ps$. Then, the radius length was subdivided into 20 segments. Thus, the grid coordinates inside the cylinder were determined by:

$$((i - 25\frac{1}{2})^2 + (j - 25\frac{1}{2})^2)^{\frac{1}{2}} \leq 20$$

For the Gaussian pulse, the program was initialized at $t = -4t_1$ $(-0.8\ ns)$ and time stepped to 4 ns (480 time steps).

Figure 3.16 shows the electric field distributions along the diameter parallel to the propagation direction of the incident pulse as the pulse propagates through the cylinder at various times $t = 0$, 0.5, 1, and 1.5 ns.

Figure 3.17 shows the electric field distributions along the diameter after the pulse reaches the far end of the cylinder at various times $t = 2.5$, 3, 3.5, and 4 ns.

For the EMP, the program was initialized at $t = 0$ ns and time stepped to 5 ns (500 time steps).

Figure 3.18 shows the electric fields along the diameter of the cylinder at various times $t = 1$, 2, 3, 4, and 5 ns. In Fig. 3.16, 3.17 and 3.18, the radius of the cylinder was normalized to 1.

3.3.4 Multi-layered Circular Cylinder of Skin, Fat, and Muscle

The outer radius of the multilayered circular cylinder was 12 cm. The outer layer was a layer of skin with a thickness of 0.2 cm. The middle layer was a layer of fat with a thickness of 1.2 cm. The core with a radius of 10.6 cm was filled with muscle. The parameters of the media were those used in section 3.2.4. The incident field was either an EMP or a Gaussian pulse of a pulse width of 1 ns.

The geometry of the cylinder relative to the grid was the same as that illustrated in Fig. 3.3 with $imax = 25$, $jmax = 50$. The cylinder axis was chosen as the line $(25\frac{1}{2}, 25\frac{1}{2}, k)$. Because the scatterer was evenly symmetric about the grid line $i = 25\frac{1}{2}$, the symmetry condition was:

$$E_z^n(26, j) = E_z^n(25, j)$$

Absorbing boundary conditions were used to truncate the grid at $i = 1$, $j = 1$, and $j = 50$.The incident wave was generated at line $j = 3$.

The node separation was chosen to be $\Delta l = 0.6\ cm$ and the time increment $\Delta t = 10\ ps$. Then, the radius length was subdivided into 20 segments. Thus, the grid coordinates inside the cylinder were determined by:

$$((i - 25\frac{1}{2})^2 + (j - 25\frac{1}{2})^2)^{\frac{1}{2}} \leq 20$$

For the Gaussian pulse, the program was initialized at $t = -4t_1$ $(-4\ ns)$ and time stepped to 5 ns (900 time steps).

Figure 3.19 shows the electric field distributions along the diameter parallel to the propagation direction of the incident pulse as the pulse begins to penetrate into the skin and fat layers. Time: $t = -2.5$, -2, -1.5, -1, and $-0.5\ ns$.

Figure 3.20 shows the electric field distributions along the diameter parallel to the propagation direction of the incident pulse as the pulse penetrates into the muscle layer. Time: $t = 0$, 1, 2, 3, and 5 ns.

For the EMP, the program was initialized at $t = 0\ ns$ and time stepped to 5 ns (500 time steps). Figure 3.21 shows the electric fields along the main diameter of the cylinder at various times $t = 1$, 2, 3, 4, and 5 ns.

In Fig. 3.19, 3.20 and 3.21, the radius of the cylinder was normalized to 1.

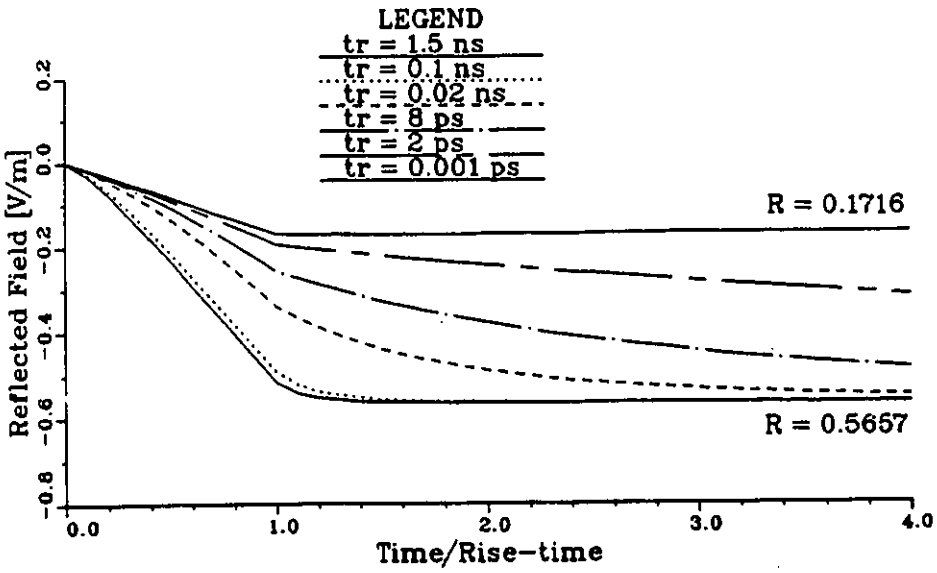

Figure 3.4: Reflected field at the interface of a Debye medium irradiated by a ramp incident field of various rise times. Medium parameters: $\epsilon_\infty = 2$, $\epsilon_0 = 13$, $\omega_0 = 10^9\ rad/s$, and $\sigma = 0$.

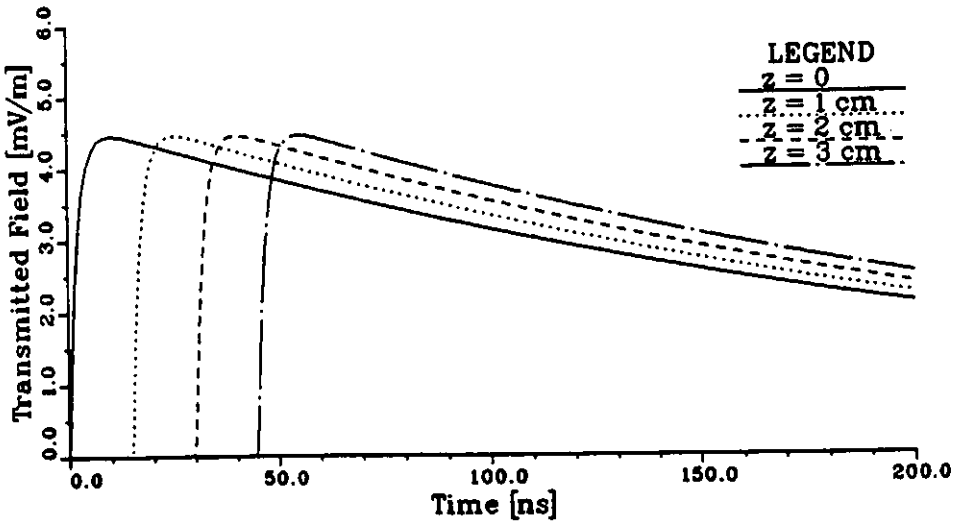

Figure 3.5: Transmitted waveforms of an EMP pulse incident on a half space filled with muscle at various depths: $z = 0, 1, 2, 3\ cm$.

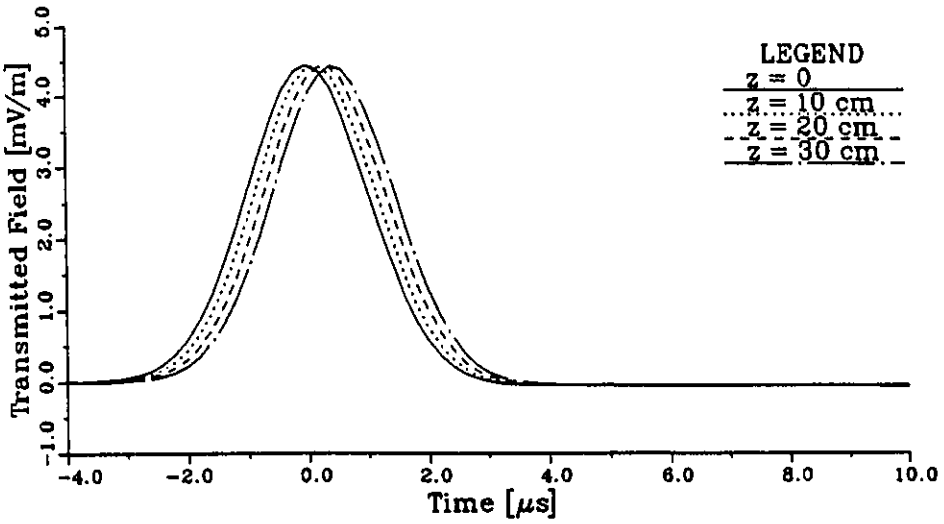

Figure 3.6: Transmitted waveforms of a Gaussian pulse incident on a half space filled with muscle at various depths: $z = 0$, 10, 20, 30 cm, for $t_1 = 1$ μs.

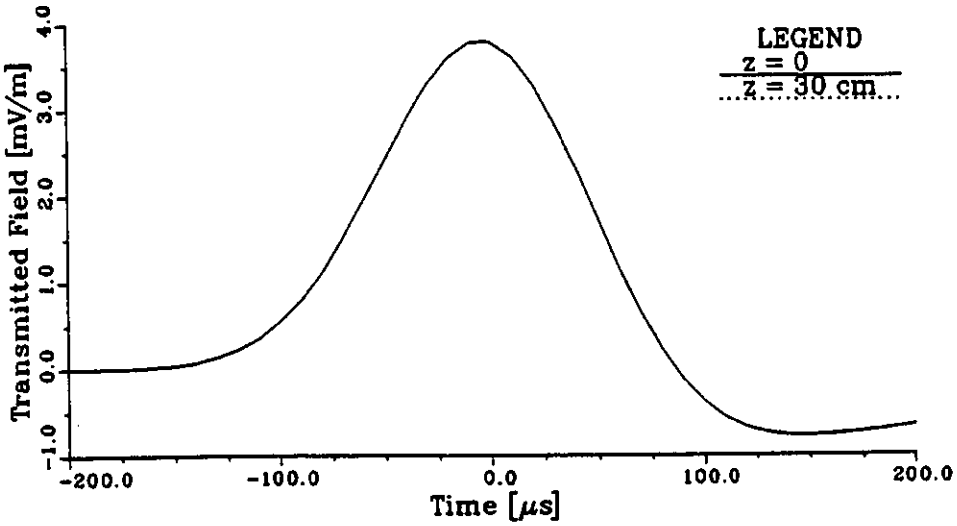

Figure 3.7: Transmitted waveforms of a Gaussian pulse incident on a half space filled with muscle at various depths: $z = 0$, 30 cm, for $t_1 = 50$ μs.

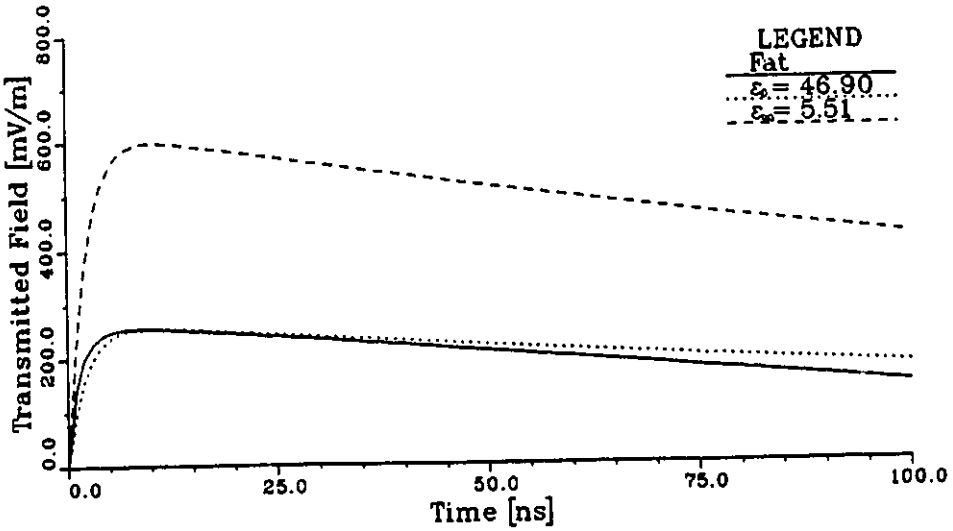

Figure 3.8: Transmitted waveforms at the interface of a half space filled with: a) Fat. b) Dielectric $\epsilon_r = \epsilon_0$. c) Dielectric $\epsilon_r = \epsilon_\infty$. The incident field was an EMP.

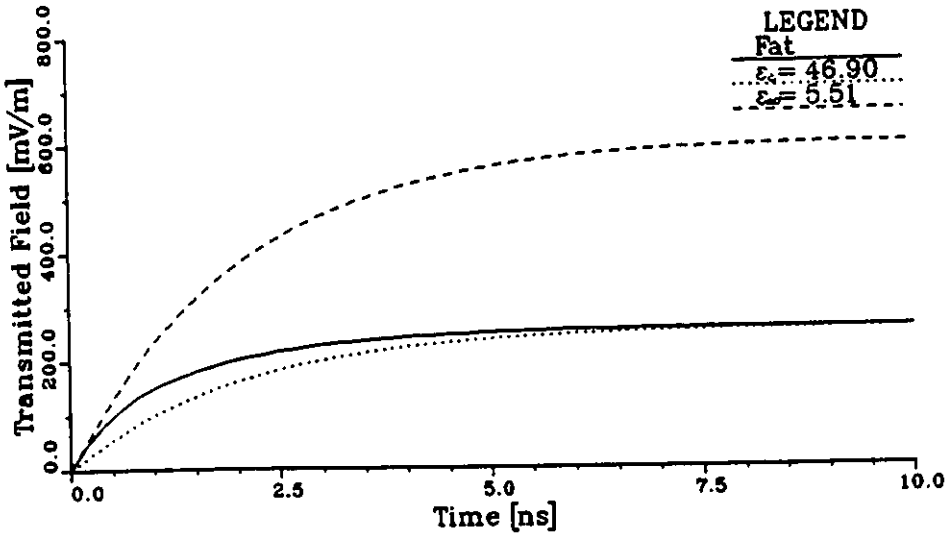

Figure 3.9: Transmitted waveforms in Fig. 3.8 at an expanded scale.

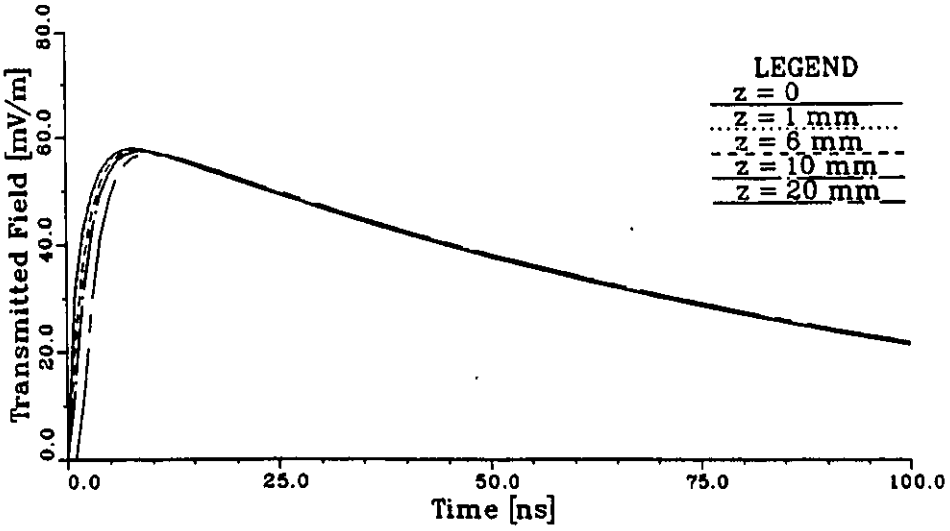

Figure 3.10: Transmitted waveforms of an EMP incident on a stratified half space filled with skin, fat, and muscle as a function of time. Time window is 100 *ns*.

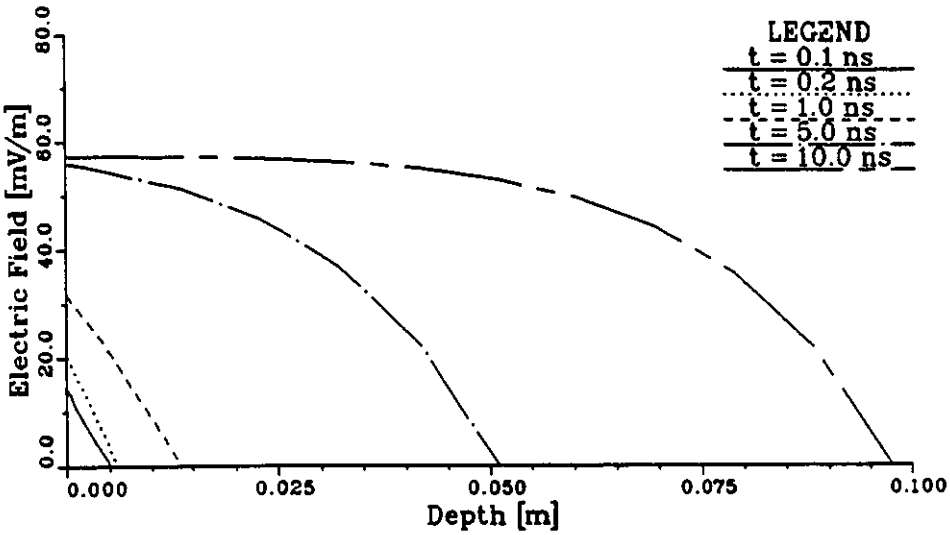

Figure 3.11: Electric field distributions in space for an EMP incident on a stratified half space filled with skin, fat, and muscle.

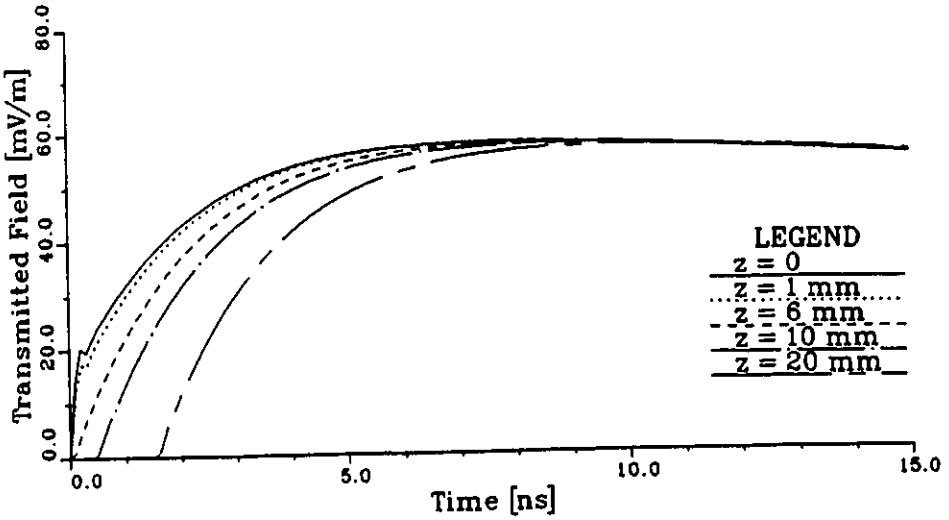

Figure 3.12: Transmitted waveforms of an EMP incident on a stratified half space filled with skin, fat, and muscle as a function of time. Time window is 15 *ns*.

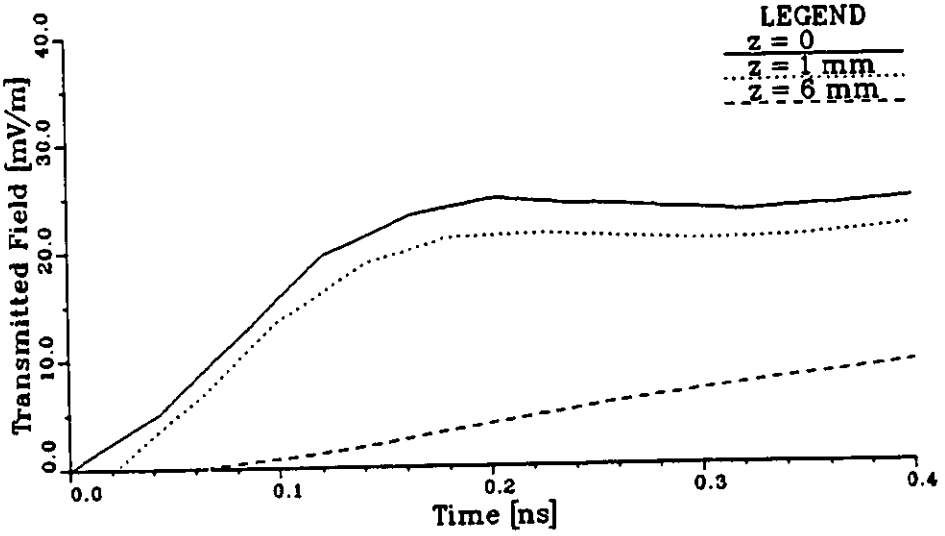

Figure 3.13: Transmitted waveforms of an EMP incident on a stratified half space filled with skin, fat, and muscle as a function of time. Time window is 0.4 *ns*.

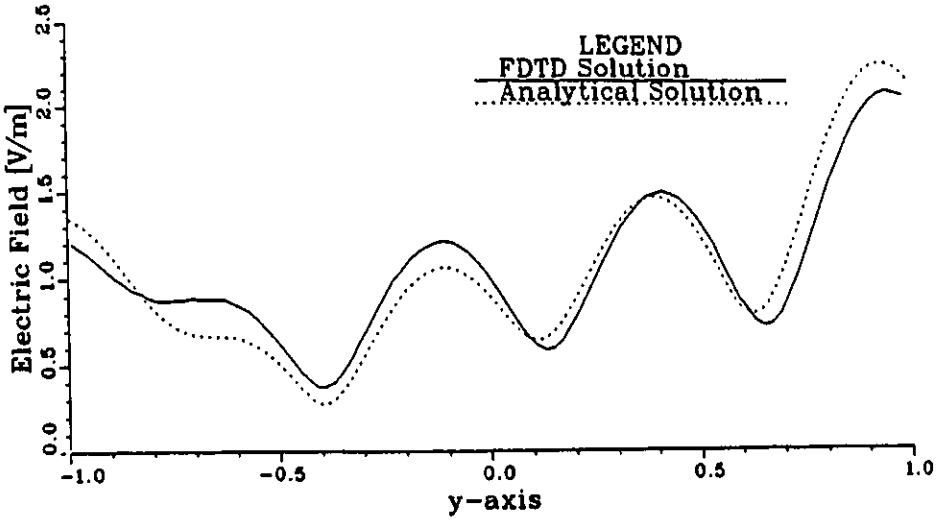

Figure 3.14: E-field distribution inside a homogeneous circular cylinder of $\epsilon_r = 4$ and along the diameter parallel to the propagation direction of the continuous incident wave. FDTD solution compared with analytical solution.

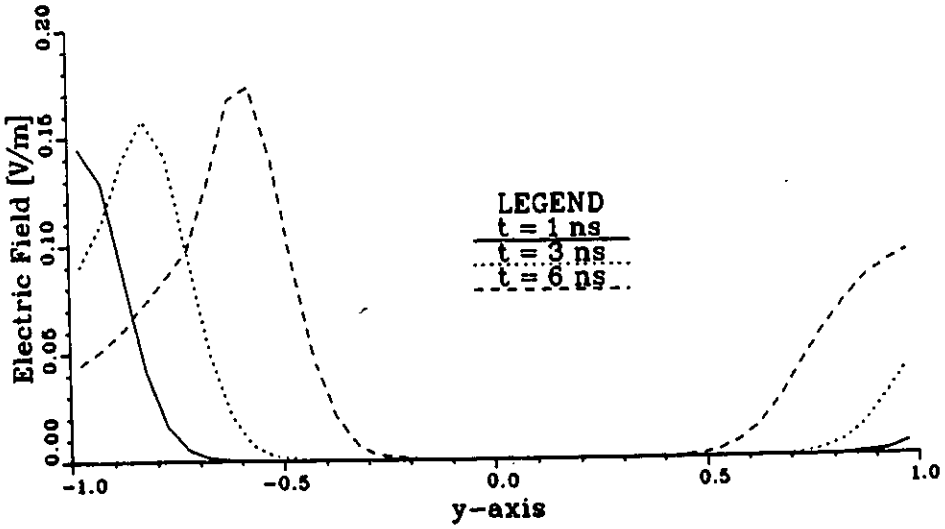

Figure 3.15: Electric field distributions along the diameter of a homogeneous circular cylinder of muscle at various times. Gaussian incident pulse of $t_1 = 1\ ns$.

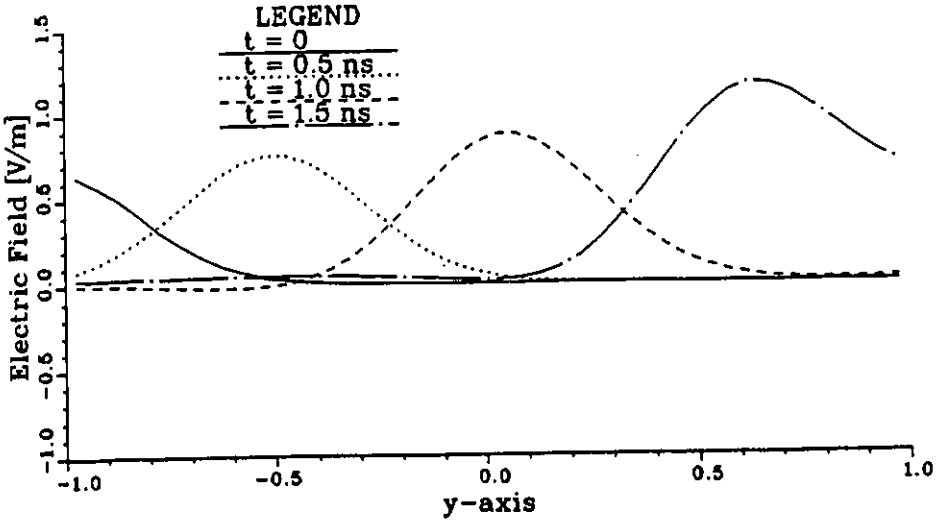

Figure 3.16: Electric field distributions along the diameter before the pulse reaches the far end of the cylinder. Fat. Gaussian incident pulse of $t_1 = 0.2\ ns$.

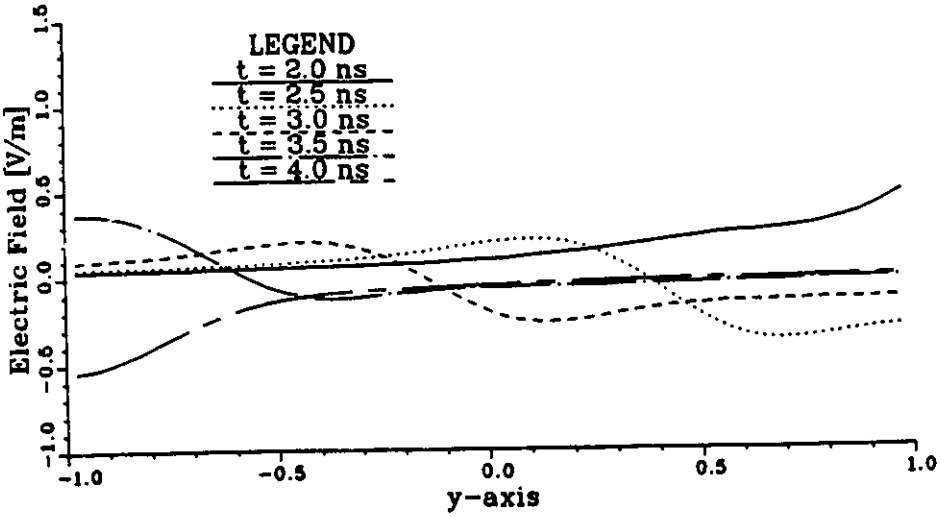

Figure 3.17: Electric field distributions along the diameter after the pulse reached the far end of the cylinder. Fat. Gaussian incident pulse of $t_1 = 0.2\ ns$.

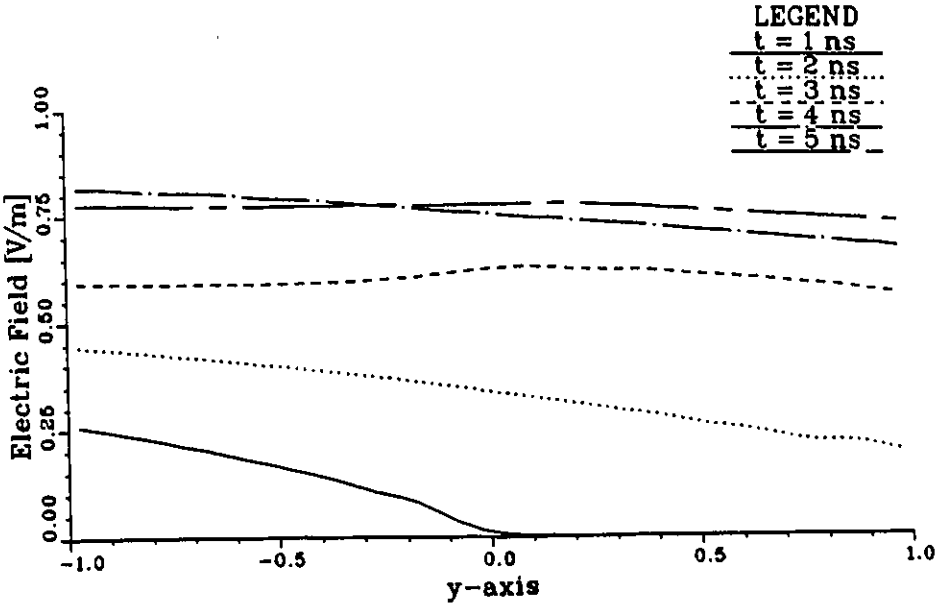

Figure 3.18: Electric field distributions along the diameter of a homogeneous circular cylinder of fat. EMP incident pulse.

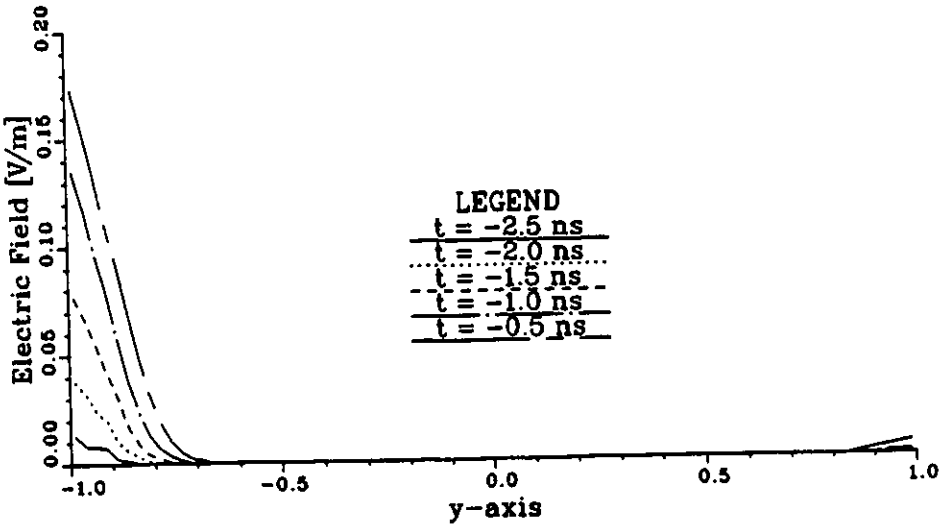

Figure 3.19: Electric field distributions along the diameter of a multilayered circular cylinder of skin,fat, and muscle. Gaussian incident pulse of $t_1 = 1\ ns$. The penetration through skin and fat layers.

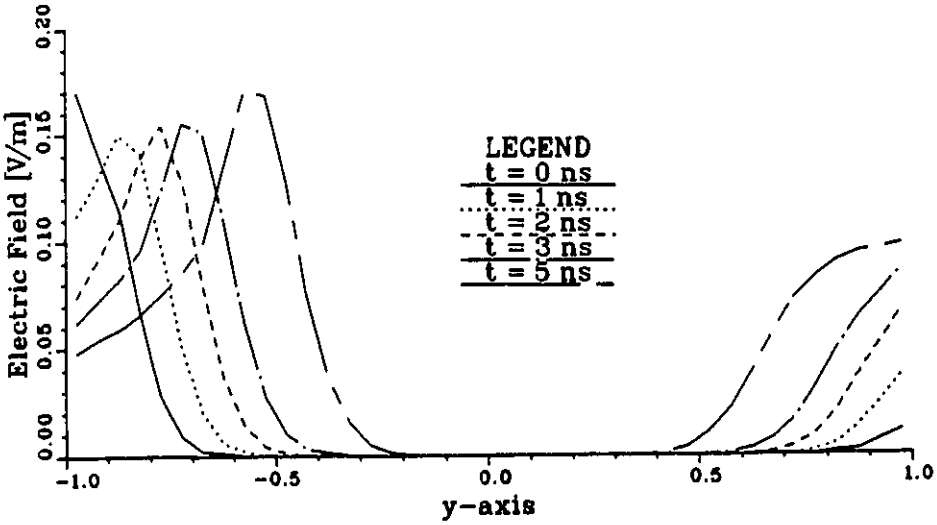

Figure 3.20: Electric field distributions along the diameter of a multilayered circular cylinder of skin,fat, and muscle. Gaussian incident pulse of $t_1 = 1\ ns$. The penetration through muscle layer.

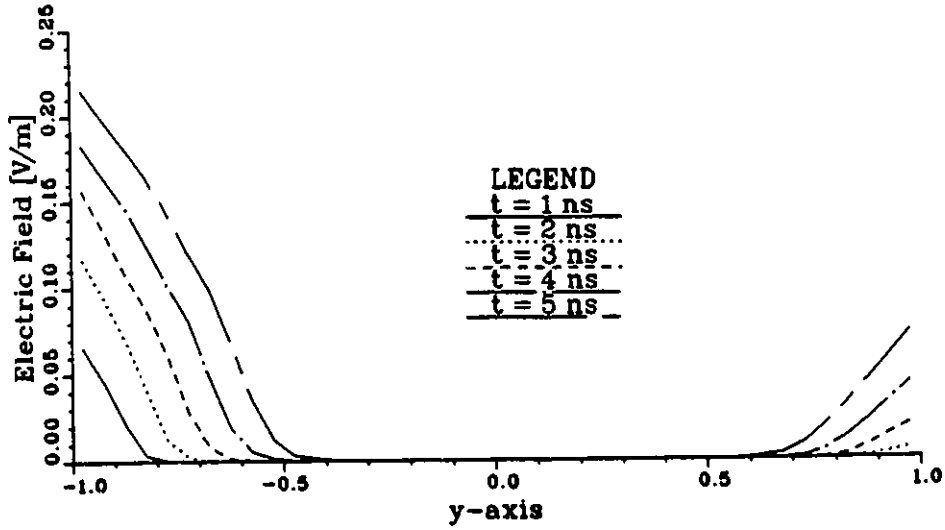

Figure 3.21: Electric field distributions along the diameter of a multilayered circular cylinder of skin, fat, and muscle. EMP incident pulse.

Chapter 4

Discussion

In this chapter, we shall discuss the results of numerical computations of the problems presented in chapter 3.

The results presented in Fig. 3.4 agree very well with those obtained by Bolomey [17] (see Appendix G for the results obtained by Bolomey.). It can be seen from Fig. 3.4 that when the rise time of the ramp incident field is small compared to the relaxation time τ_0 of the medium, the medium behaves as a dielectric of relative permittivity equal to ϵ_∞. On the other hand, when the rise time is large compared to the relaxation time, the medium behaves as a dielectric of relative permittivity equal to ϵ_0. When the rise time is comparable with the relaxation time, the waveform is distorted. Thus, the dispersion occurs. These observations can be justified by putting the permittivity of the dispersive medium equal to ϵ_∞ or ϵ_0 and calculating the reflection coefficients at the interface in each case. The reflection coefficient is given by:

$$R = \frac{\sqrt{\epsilon_r} - 1}{\sqrt{\epsilon_r} + 1}$$

Thus, for $\epsilon_r = \epsilon_0 = 13$, the reflection coefficient is 0.5657 which corresponds to the curve $t_r = 1.5\ ns$ in Fig. 3.4. For $\epsilon_r = \epsilon_\infty = 2$, the reflection coefficient is 0.1716 which corresponds to the curve $t_r = 0.001\ ps$ in Fig. 3.4.

The results presented in Fig. 3.5 confirm these observations. Indeed, the waveforms in this case were not distorted because the time window used (0.2 μs) was small compared to the relaxation time of muscle (12.5 μs). The muscle then behaved as a dielectric of relative permittivity equal to

$\epsilon_\infty = 0.2 \times 10^6$. The transmission coefficient in this case is given by:

$$T = \frac{2}{\sqrt{\epsilon_\infty} + 1}$$

which is equal to 4.46×10^{-3} corresponding to the peaks of the transmitted waveforms in Fig. 3.5.

The results presented in Fig. 3.6 and 3.7 agree very well with those obtained by Lin [11] (see Appendix G for the results obtained by Lin.). In Fig. 3.6, the muscle behaved as a dielectric with $\epsilon_r = 0.2 \times 10^6$ because the pulse width was much shorter than the relaxation time of muscle. In Fig. 3.7, the muscle behaved as a dielectric with $\epsilon_r = 2.55 \times 10^6$ because the pulse width was much longer than the relaxation time of muscle. Also in Fig. 3.7, one notices that although the incident pulse was entirely positive, the transmitted pulse had both positive and negative contributions. The negative contribution may be related to the reflection at the interface.

Figures 3.8 and 3.9 show the transmitted waveform at the interface for an EMP incident on a homogeneous half space filled with fat. Similar waveforms with fat replaced by dielectrics of relative permittivities equal to $\epsilon_\infty = 5.51$ and $\epsilon_0 = 46.9$ were also introduced to demonstrate the short and long time behavior of fat for an EMP. In Fig. 3.9, the dispersion of the transmitted pulse can be observed during the time window 0 to 10 ns.

Figures 3.10 and 3.11 present the transmitted waveforms and the penetration of an EMP incident in a stratified half space filled with skin, fat, and muscle. The waveform at $z = 0$ was the electric field at the interface of the air and the skin layer. The waveform at $z = 1$ mm was the electric field at the interface of the skin layer and the fat layer. The waveform at $z = 6$ mm was the electric field at a node inside the fat layer. The waveforms at $z = 10$ mm and $z = 20$ mm were the electric fields at nodes inside the muscle layer.

The results presented in Fig. 3.12 and 3.13 show the multiple reflections of the electric field as it has just penetrated into the stratified half space filled with skin, fat, and muscle.

The results presented in Fig. 3.14 show relatively good agreement between the FDTD solution and the analytical solution [21]. The agreement deteriorates near the interface.

The results presented in Fig. 3.15 show the penetration of a Gaussian pulse incident on a homogeneous circular cylinder of muscle. One can observe

the increase of the pulse strength as the pulse propagates toward the center of the cylinder. The cause for this increase may be the superimposition of the electric fields penetrating from all directions into the cylinder. One can also observe the build-up of the electric field near the far end of the cylinder.

The results presented in Fig. 3.16 and 3.17 show the propagation of a Gaussian pulse incident on a homogeneous circular cylinder filled with fat. In Fig. 3.16, one can observe that the pulse amplitude increases as the pulse propagates toward the far end of the cylinder. In Fig. 3.17, the electric field distributions along the diameter after the pulse has reached the far end of the cylinder were observed at various times. From Fig. 3.16 and 3.17, one can conclude that the electric field inside the cylinder reaches maximum near the far end of the cylinder when the pulse has just arrived there.

The results presented in Fig. 3.18 show the penetration of an EMP incident on a homogeneous circular cylinder of fat. It can be seen from the figure that the maximum pulse amplitude occurs after the pulse is reflected back to the far end for the second time.

Figure 3.19 shows the formation of the transmitted pulse for a Gaussian pulse incident on a multilayered circular cylinder of skin, fat, and muscle. It can be seen that as the transmitted pulse is formed at the front end of the cylinder, the electric field at the rear end of the cylinder is also building up.

A comparison between the results in Fig. 3.20 and those in Fig. 3.15 indicates that the electric field penetrations into muscle material in both cases are almost the same in spite of the presence of the fat and skin layers in the problem presented in Fig. 3.20.

Figure 3.21 shows the electric field penetration of an EMP incident on a stratified circular cylinder filled with skin, fat, and muscle. Again, the electric field at the far end of the cylinder begins to build-up early and reaches approximately one third of the transmitted field at the front end at $t = 5\ ns$.

There are three main sources of error in the FDTD method. The first is the imperfection of the absorbing boundary conditions. The second is the stepped-edge approximation of the boundary of the cylinder. And, the third is the numerical dispersion. Numerical dispersion is the distortion of the pulse due to the change of the phase velocity with modal wavelength, direction of propagation, and the mesh resolution. Numerical dispersion reduces subtantially with fine resolution mesh [38]. Thus, to improve the accuracy of the solution, one can increase the resolution of the mesh. However, larger mesh size requires more computer time and memory. Overall, the FDTD solution may be considered accurate up to 500 time steps for the mesh size of (25×50).

In general, the FDTD method presented in chapter 2 is very powerful. It allows modeling of arbitrary-shaped structures and is easy to implement. In addition, the method requires relative little computer time and memory. One disadvantage of the method is that all the nodes of the mesh have to be calculated regardless of whether the node is needed or not. Besides, the imperfection of the absorbing boundary conditions does not allow the method to be used to analyse the propagation of extremely short pulses in high permittivity media. Huge number of time steps would be required to allow the observation of the pulse propagation.

Chapter 5

Conclusions

The primary objective of this study was to investigate the propagation of pulsed electromagnetic fields in dispersive dielectrics. The FDTD technique used for solving one and two-dimensional problems of propagation of pulsed electromagnetic fields has been presented. Many problems of propagation with different types of incident pulses, various kinds of dispersive media of different geometries have been investigated.

Several new results have been obtained. For one-dimensional problem, the electric fields in stratified half space of skin, fat, and muscle were computed. For two-dimensional problem, the electric fields in homogeneous circular cylinder of muscle, homogeneous circular cylinder of fat, and multi-layered circular cylinder of skin, fat, and muscle were also computed.

The results obtained indicate that the pulse does not disperse when the pulse width is very small or very large compared to the relaxation time of the medium. For two-dimensional problems, the results suggest that the pulsed electromagnetic fields penetrate into a dispersive dielectric cylinder not only from the direction of propagation of the incident pulse but also from all other directions. Therefore, in many cases, the maximum pulse amplitude is reached when the pulse has penetrated deep inside the cylinder.

In conclusion, the FDTD technique is applicable to most of one and two-dimensional problems. However, the technique is not suitable for extremely short pulses propagating in a medium of very high permittivity because a huge number of time steps would be required to allow the observation of the pulse propagation. Further study of the absorbing boundary conditions is needed to overcome this limitation.

Appendix A

Derivatives of Electric flux

The electric flux density is:

$$\vec{D}(x,y,z,t) = \int_{-\infty}^{\infty} \epsilon(t-\beta)\vec{E}(x,y,z,\beta)d\beta$$

$$\vec{D}(x,y,z,t) = \epsilon_\infty \vec{E}(x,y,z,t) + \frac{\epsilon_0 - \epsilon_\infty}{\tau_0} \int_{-\infty}^{\infty} e^{-\frac{t-\beta}{\tau_0}} u(t-\beta)\vec{E}(x,y,z,\beta)d\beta$$

Suppose:

$$\vec{D}(x,y,z,t) = D_x(x,y,z,t)\vec{x}$$

Then:

$$D_x(x,y,z,t) = \epsilon_\infty E_x(x,y,z,t) + \frac{\epsilon_0 - \epsilon_\infty}{\tau_0} \int_{-\infty}^{\infty} e^{-\frac{t-\beta}{\tau_0}} u(t-\beta)E_x(x,y,z,\beta)d\beta$$

Take derivative with respect to t on both sides:

$$\frac{\partial D_x(x,y,z,t)}{\partial t} = \epsilon_\infty \frac{\partial E_x(x,y,z,t)}{\partial t} + \frac{\epsilon_0 - \epsilon_\infty}{\tau_0} \int_{-\infty}^{\infty} \frac{\partial}{\partial t}\left\{e^{-\frac{t-\beta}{\tau_0}} u(t-\beta)E_x(x,y,z,\beta)\right\} d\beta$$

$$\frac{\partial D_x(x,y,z,t)}{\partial t} = \epsilon_\infty \frac{\partial E_x(x,y,z,t)}{\partial t} + \frac{\epsilon_0 - \epsilon_\infty}{\tau_0} \int_{-\infty}^{\infty} \left\{ \delta(t-\beta) - \frac{1}{\tau_0} u(t-\beta) \right\} e^{-\frac{t-\beta}{\tau_0}} E_x(x,y,z,\beta) d\beta$$

$$\frac{\partial D_x(x,y,z,t)}{\partial t} = \epsilon_\infty \frac{\partial E_x(x,y,z,t)}{\partial t} + \frac{\epsilon_0 - \epsilon_\infty}{\tau_0} E_x(x,y,z,t) - \frac{\epsilon_0 - \epsilon_\infty}{\tau_0^2} \int_{-\infty}^{\infty} e^{-\frac{t-\beta}{\tau_0}} u(t-\beta) E_x(x,y,z,\beta) d\beta$$

Take second derivative with respect to t:

$$\frac{\partial^2 D_x(x,y,z,t)}{\partial t^2} = \epsilon_\infty \frac{\partial^2 E_x(x,y,z,t)}{\partial t^2} + \frac{\epsilon_0 - \epsilon_\infty}{\tau_0} \frac{\partial E_x(x,y,z,t)}{\delta t} - \frac{\epsilon_0 - \epsilon_\infty}{\tau_0^2} \int_{-\infty}^{\infty} \frac{\partial}{\partial t} \left\{ e^{-\frac{t-\beta}{\tau_0}} u(t-\beta) \right\} E_x(x,y,z,\beta) d\beta$$

$$\frac{\partial^2 D_x(x,y,z,t)}{\partial t^2} = \epsilon_\infty \frac{\partial^2 E_x(x,y,z,t)}{\partial t^2} + \frac{\epsilon_0 - \epsilon_\infty}{\tau_0} \frac{\partial E_x(x,y,z,t)}{\partial t} - \frac{\epsilon_0 - \epsilon_\infty}{\tau_0^2} E_x(x,y,z,t) + \frac{\epsilon_0 - \epsilon_\infty}{\tau_0^3} \Delta t S_x(x,y,z,t)$$

where

$$S_x(x,y,z,t) = \frac{1}{\Delta t} \int_{-\infty}^{\infty} e^{-\frac{t-\beta}{\tau_0}} u(t-\beta) E_x(x,y,z,\beta) d\beta$$

$$S_x(x,y,z,t) = \frac{1}{\Delta t} \int_{0}^{t} e^{-\frac{t-\beta}{\tau_0}} E_x(x,y,z,\beta) d\beta$$

Appendix B

Stability Criterion

Suppose we have the wave equation:

$$\frac{\partial^2 E}{\partial t^2} - c^2 \frac{\partial^2 E}{\partial z^2} = 0$$

Consider the Taylor series expansions:

$$E(z+\Delta z) = E(z) + \frac{\Delta z}{1}\frac{\partial E(z)}{\partial z} + \frac{\Delta z^2}{2}\frac{\partial^2 E(z)}{\partial z^2} + \frac{\Delta z^3}{6}\frac{\partial^3 E(z)}{\partial z^3} + \frac{\Delta z^4}{24}\frac{\partial^4 E(z)}{\partial z^4} + \cdots$$

$$E(z-\Delta z) = E(z) - \frac{\Delta z}{1}\frac{\partial E(z)}{\partial z} + \frac{\Delta z^2}{2}\frac{\partial^2 E(z)}{\partial z^2} - \frac{\Delta z^3}{6}\frac{\partial^3 E(z)}{\partial z^3} + \frac{\Delta z^4}{24}\frac{\partial^4 E(z)}{\partial z^4} - \cdots$$

or

$$E(z+\Delta z) + E(z-\Delta z) = 2E(z) + \Delta z^2 \frac{\partial^2 E(z)}{\partial z^2} + \frac{\Delta z^4}{12}\frac{\partial^4 E(z)}{\partial z^4} + \cdots$$

$$\frac{\partial^2 E(z)}{\partial z^2} = \frac{E(z+\Delta z) - 2E(z) + E(z-\Delta z)}{\Delta z^2} - \frac{\Delta z^2}{12}\frac{\partial^4 E(z)}{\partial z^4} - \cdots$$

A similar expression can be obtained for the time variable t.

Substitute $\frac{\partial^2 E}{\partial z^2}$ and $\frac{\partial^2 E}{\partial t^2}$ into the wave equation and rearrange, we have:

$$E_i^{n+1} = -E_i^{n-1} + 2\left[1 - \left(\frac{c\Delta t}{\Delta z}\right)^2\right] E_i^n + \left(\frac{c\Delta t}{\Delta z}\right)^2 \left[E_{i+1}^n + E_{i-1}^n\right] + T \quad \text{(B.1)}$$

where T is truncation error:

$$T = \frac{(c\Delta t\Delta z)^2}{12}\left[\frac{1}{c^4}\left(\frac{c\Delta t}{\Delta z}\right)^2 \frac{\partial^4 E(z)}{\partial t^4} - \frac{\partial^4 E(z)}{\partial z^4}\right] + \text{higher order terms}$$

To find the stability criterion, let the solution of (B.1) be the form:

$$E_i^n = \beta^n e^{j\alpha i}$$

where α and β are constant with α real.
Since number of time steps n can be increased without bound, β must be less than 1 for a stable solution.
Substitute E_i^n into (B.1), we have

$$\begin{aligned}\beta^{n+1}e^{j\alpha i} &= -\beta^{n-1}e^{j\alpha i} + 2\left[1 - \left(\frac{c\Delta t}{\Delta z}\right)^2\right]\beta^n e^{j\alpha i} \\ &\quad + \left(\frac{c\Delta t}{\Delta z}\right)^2\left(\beta^n e^{j\alpha(i+1)} + \beta^n e^{j\alpha(i-1)}\right)\end{aligned}$$

Divide both sides by $\beta^{n-1}e^{j\alpha i}$, we have:

$$\begin{aligned}\beta^2 &= -1 + 2\left[1 - \left(\frac{c\Delta t}{\Delta z}\right)^2\right]\beta + \left(\frac{c\Delta t}{\Delta z}\right)^2\beta\left(e^{j\alpha} + e^{-j\alpha}\right) \\ \beta^2 &= -1 + 2\left[1 - \left(\frac{c\Delta t}{\Delta z}\right)^2\right]\beta + 2\left(\frac{c\Delta t}{\Delta z}\right)^2 cos(\alpha)\beta \\ \beta^2 &= -1 + 2\left[1 - \left(\frac{c\Delta t}{\Delta z}\right)^2(1 - cos(\alpha))\right]\beta\end{aligned}$$

or

$$\beta^2 - 2\left[1 - 2\left(\frac{c\Delta t}{\Delta z}\right)^2 sin^2(\frac{\alpha}{2})\right]\beta + 1 = 0$$

Let the roots of the above equation be β_1 and β_2, then:

$$\beta_1 + \beta_2 = 2\left[1 - 2\left(\frac{c\Delta t}{\Delta z}\right)^2 sin^2(\frac{\alpha}{2})\right]$$

The requirements $|\beta_1| \leq 1$ and $|\beta_2| \leq 1$ imply:

$$|1 - 2\left(\frac{c\Delta t}{\Delta z}\right)^2 sin^2(\frac{\alpha}{2})| \leq 1$$

or

$$\left| \left(\frac{c\Delta t}{\Delta z}\right)^2 sin^2(\frac{\alpha}{2}) \right| \leq 1$$

since α is real, we have:

$$\left(\frac{c\Delta t}{\Delta z}\right) sin(\frac{\alpha}{2}) \leq 1$$

or

$$\frac{c\Delta t}{\Delta z} \leq 1$$

This is the stability criterion for all real α.
If $\Delta z = c\Delta t$ then

$$\begin{aligned} T &= \frac{(c\Delta t \Delta z)^2}{12}\left[\frac{1}{c^4}\frac{\partial^4 E(z)}{\partial t^4} - \frac{\partial^4 E(z)}{\partial z^4}\right] + \text{higher order terms} \\ &= \frac{(c\Delta t \Delta z)^2}{12}\left[\frac{1}{c^2}\frac{\partial^2 E(z)}{\partial t^2} - \frac{\partial^2 E(z)}{\partial z^2}\right]\left[\frac{1}{c^2}\frac{\partial^2 E(}{\partial} \quad \cdot \frac{\partial^2 E(z)}{\partial z^2}\right] \\ &\quad + \text{higher order terms} \end{aligned}$$

Thus, the truncation error reduces to zero.

Appendix C

Computer Program for Stratified Half Space of Lossy Dispersive Media. The FDTD Solution.

```
THIS PROGRAM COMPUTES THE REFLECTED WAVEFORM OF AN
EMP PULSE NORMALLY INCIDENT TO A N-LAYERED DISPERSIVE
DIELECTRIC HALF SPACE ASSUMES A DEBYE MODEL
C
C ND = THICKNESS ( NUMBER OF SPATIAL SEGMENTS )
C NSTEP1 = NUMBER OF TIME STEPS TO BE CALCULATED
C W0DT = W0 x DT
C EPS = RELATIVE DIELECTRIC CONSTANT OF AIR
C EPS0 = RELATIVE LOW FREQ. DIELECTRIC
C EPSN = RELATIVE HIGH FREQ. DIELECTRIC
C COND0 = LOW FREQ. CONDUCTIVITY
C
INTEGER*4 ND(5),NZ(10),NJ(10),JMPZ(5)
INTEGER*4 NEND,NEND1,NSTEP1,IEND,IEND1,IBOUND
REAL*8 F0(10000),F1(10000),F2(10000),SUM(10000),SUM2(5),
REAL*8 Q1(5),Q2(5),Q3(5),Q4(5),Q5(5),Q6(5),S1(5),S2(5), S3(5),S4(5),
REAL*8 S5(5),DZ(5),EPS21(5),G(5),CONDR(5),THICK(5)
REAL*8 E0,C0,EPS,T,DT,EPSMAX,EPS0,EPSN,COND0,W0,W0DT,A,
```

```
REAL*8 TEMP,FI0,FI1,FI2,DEPTH,TIME,V,Z,PI
CHARACTER*10 FNAME
E0(T)=1.05016D3*(DEXP(-4.D6*T)-DEXP(-4.76D8*T))
PI=4.D0*DATAN(1.D0)
C0=2.997925D8
EPS=1.0D0
TYPE *, ' ENTER NL( ≤ 5 ), DT, NSTEP1, JMPN'
ACCEPT *, NL,DT,NSTEP1,JMPN
TYPE *, ' ENTER NSP(≤ 10) and NTI(≤ 10)'
ACCEPT *, NSP, NTI
NEND=2
TYPE *, ' INTERFACE 1 AT SPATIAL POINT :',NEND
DO J=1,NL
TYPE 3, J
ACCEPT *, EPS0,EPSN,COND0,THICK(J),W0
IF(NTI.GT.0) THEN
TYPE *, ' ENTER JMPZ FOR LAYER',J
ACCEPT *, JMPZ(J)
ENDIF
V=C0/DSQRT(EPSN)
DZ(J)=V*DT
ND(J)=INT(THICK(J)/DZ(J))
TYPE *, ' LAYER',J,' HAS',ND(J),' SPATIAL POINTS'
W0DT=W0*DT
G(J)=DEXP(-W0DT)
EPS21(J)=DSQRT(EPS/EPSN)
A=(EPS0-EPSN)/EPSN
CONDR(J)=COND0*DT/EPSN+A*W0DT
Q1(J)=1.D0+0.5D0*CONDR(J)
Q2(J)=1.D0-0.5D0*CONDR(J)
Q3(J)=A*W0DT*W0DT
Q4(J)=Q3(J)*W0DT
Q5(J)=(EPS21(J)+Q1(J))/2.D0
Q6(J)=(EPS21(J)+Q2(J))/2.D0
IF(J.NE.1) THEN
TEMP=EPS21(J)*CONDR(J-1)+CONDR(J)
S1(J)=0.5D0*(1.D0+EPS21(J)+0.5D0*TEMP)
```

```
S2(J)=0.5D0*(1.D0+EPS21(J)-0.5D0*TEMP)
S3(J)=(EPS21(J)*Q3(J-1)+Q3(J))/2.D0
S4(J)=EPS21(J)*Q4(J-1)/2.D0
S5(J)=Q4(J)/2.D0
NEND=NEND+ND(J-1)
TYPE *, ' INTERFACE',J,' AT SPATIAL POINT :',NEND
ENDIF
EPS=EPSN
ENDDO
C
DO I=1,NSP
TYPE *, ' ENTER DEPTH FOR SPATIAL POINT NUMBER',I
ACCEPT *, DEPTH
J=0
NZ(I)=0
10 J=J+1
TEMP=DEPTH
DEPTH=DEPTH-THICK(J)
IF(DEPTH.LT.0.D0) THEN
NZ(I)=NZ(I)+INT(TEMP/DZ(J))+2
ELSE
NZ(I)=NZ(I)+ND(J)
GOTO 10
ENDIF
TYPE *, ' THE POINT NUMBER IS',NZ(I),' IN LAYER',J
TYPE *, ' ENTER FILE NAME'
ACCEPT 6, FNAME
OPEN(UNIT=I,NAME=FNAME,TYPE='NEW')
WRITE(I,1) T*1.D9,F1(NZ(I))
ENDDO
DO I=1,NTI
TYPE *, 'ENTER TIME FOR TIME POINT NUMBER',I
ACCEPT *, TIME
TYPE *, ' ENTER FILE NAME'
ACCEPT 6, FNAME
NJ(I)=INT(TIME/DT)+1
OPEN(UNIT=NSP+I,NAME=FNAME,TYPE='NEW')
```

```
ENDDO
C
TYPE 5, NZ(NSP)-NEND
ACCEPT *, NEND1
NEND=NEND+NEND1
TYPE *, ' THE LAST SPATIAL POINT WHICH IS ACCURATE IS',NEND
IEND=(NSTEP1+NEND)/2+1
TYPE *, ' NUMBER OF SPATIAL POINTS USED IS',IEND
IEND1=IEND-1
DO I=2,IEND
SUM(I)=0.D0
F0(I)=0.D0
F1(I)=0.D0
ENDDO
C
C INCIDENT FIELDS TO THE AIR/DIELECTRIC INTERFACE AT T=0.0

C
J=1
T=0.D0
FI0=0.D0
FI1=0.D0
F0(1)=FI0
F1(1)=FI1
F1(2)=EPS21(J)*F1(1)/Q5(J)
C
C FINITE DIFFERENCE SOLUTIONS START HERE
C
L=0
DO 100 N=2,NSTEP1
T=T+DT
FI2=E0(T)
J=1
IBOUND=ND(J)+2
F2(1)=FI2+F1(2)-FI0
FI0=FI1
FI1=FI2
```

```
C
C I=2 IS THE AIR/DIELECTRIC INTERFACE
C
I=2
SUM(2)=SUM(2)*G(1)+(F0(2)*G(1)+F1(2))/2.D0
F2(2)=(-Q6(1)*F0(2)+F1(3)+EPS21(1)*F1(1)+0.5D0*(Q3(1)*F1(2)
-Q4(1)*SUM(2)))/Q5(1)
C
C EFFICIENT MOVING TIME WINDOW CALCULATIONS ADOPTED
C
Z=0.D0
IF(N.EQ.NJ(L+1)) THEN
L=L+1
WRITE(NSP+L,1) Z,F2(2)
ENDIF
IF(N.LT.IEND1) MOVING=N+1
IF(N.GT.IEND1) MOVING=N-1
DO 20 I=3,MOVING
Z=Z+DZ(J)
SUM(I)=SUM(I)*G(J)+(F0(I)*G(J)+F1(I))/2.D0
IF(I.EQ.IBOUND) THEN
J=J+1
SUM2(J)=SUM2(J)*G(J)+(F0(I)*G(J)+F1(I))/2.D0
F2(I)=(-S2(J)*F0(I)+EPS21(J)*F1(I-1)+F1(I+1)
+S3(J)*F1(I)-S4(J)*SUM(I)-S5(J)*SUM2(J))/S1(J)
IBOUND=IBOUND+ND(J)
ELSE
F2(I)=(-Q2(J)*F0(I)+F1(I-1)+F1(I+1)
+Q3(J)*F1(I)-Q4(J)*SUM(I))/Q1(J)
ENDIF
IF((N.EQ.NJ(L)).AND.(MOD(I-2,JMPZ(J)).EQ.0)
.AND.(I.LE.NEND)) WRITE(NSP+L,1) Z,F2(I)
20 CONTINUE
C
C UPDATE THE FIELDS AT A NEW TIME STEPS
C
IF(MOD(N-1,JMPN).EQ.0) THEN
```

```
DO K=1,NSP
WRITE(K,1) T*1.D9,F2(NZ(K))
ENDDO
ENDIF
DO I=1,MOVING
F0(I)=F1(I)
F1(I)=F2(I)
ENDDO
100 CONTINUE
DO I=1,NSP+NTI
WRITE(I,1) -999.,-999.
CLOSE(UNIT=I)
ENDDO
1 FORMAT(2(5X,F10.4))
3 FORMAT(' Enter EPS0, EPSN, COND0,THICK ,and W0 for layer',I4)
5 FORMAT(' Enter number of points after last interface ( ≥ ',I6,')')
6 FORMAT(A20)
STOP
END
```

Appendix D

Computer Program for Multi-layered Circular Cylinder of Lossy Dielectric Exposed to a Continuous Plane Wave. The Theoretical Solution.

```
THIS PROGRAM CALCULATES THE THEORETICAL SOLUTION FOR
A LOSSY DIELECTRIC MULTILAYER CIRCULAR CYLINDER OF IN-
FINITE LENGTH EXPOSED TO A PLANE WAVE INCIDENT NOR-
MALLY TO THE AXIS CASE (E-FIELD // Z-AXIS)
C
COMPLEX*16 A(2,2),B(2),U,PHI,CI,CR,CZ,CM(2,5,20),TERM
COMPLEX*16 JN(20,300),YN(20,300),JN1(20,300),YN1(20,300)
COMPLEX*16 DJN1(20,10),DYN1(20,10),DJN(20,10),DYN(20,10)
COMPLEX*16 KR1(300),KR2(300)
COMPLEX*16 KL(5),ER(5),K0,X1(5),X(5)
REAL*8 RA(5),LAMDA(5),R(300),KL0(5)
REAL*8 FREQ,W,C,EPS0,MU0,PI,DR,THE,D,Q,LAMDA0,ER1,ER2
INTEGER NR(5),NPOINT(5)
```

```
C
PI=4.D0*DATAN(1.D0)
CI=DCMPLX(0.D0,1.D0)
CR=DCMPLX(1.D0,0.D0)
CZ=DCMPLX(0.D0,0.D0)
C=2.997925D8
MU0=PI*4.D-7
EPS0=1.D0/(MU0*C**2)
NL=1
TYPE *, ' NUMBER OF LAYERS IS',NL
TYPE *, ' PLEASE ADJUST THE SIZE OF METRICE [A] , [B] TO',2*NL
FREQ=2.5D9
W=2.D0*PI*FREQ
LAMDA0=C/FREQ
K0=W/C
D=0.D0
R(1)=0.D0
TYPE *, ' ENTER NUMBER OF TERMS M FOR Cm'
ACCEPT *, N
DO L=1,NL
TYPE 5, L
ACCEPT *, ER1,ER2,RA(L),NR(L)
ER(L)=DCMPLX(ER1,-ER2)
RA(L)=RA(L)*LAMDA0
KL(L)=W*CDSQRT(MU0*EPS0*ER(L))
IF(L.EQ.1) THEN
DR=RA(L)/NR(L)
NP=1
KR1(NP)=0.D0
DO I=1,NR(L)
NP=NP+1
D=D+DR
R(NP)=D
KR1(NP)=KL(L)*R(NP)
ENDDO
NP1=NP
NP2=0
```

```
ELSE
DR=(RA(L)-RA(L-1))/NR(L)
DO I=1,NR(L)
NP=NP+1
NP2=NP2+1
D=D+DR
R(NP)=D
KR2(NP2)=KL(L)*R(NP)
ENDDO
ENDIF
NPOINT(L)=NP
ENDDO
KL(NL+1)=K0
C
C CALCULATE FOURIER COEFFICIENT CM'S
C
DO L=1,NL
X(L)=KL(L)*RA(L)
X1(L)=KL(L+1)*RA(L)
ENDDO
CALL BESSEL(N+1,JN,YN,X,NL)
CALL BESSEL(N+1,JN1,YN1,X1,NL)
DO L=1,NL
DJN(1,L)=-JN(2,L)
DYN(1,L)=-YN(2,L)
DJN1(1,L)=-JN1(2,L)
DYN1(1,L)=-YN1(2,L)
DO I=2,N
DJN(I,L)=(JN(I-1,L)-JN(I+1,L))/2.D0
DYN(I,L)=(YN(I-1,L)-YN(I+1,L))/2.D0
DJN1(I,L)=(JN1(I-1,L)-JN1(I+1,L))/2.D0
DYN1(I,L)=(YN1(I-1,L)-YN1(I+1,L))/2.D0
ENDDO
ENDDO
C
C COMPUTE METRIX [A] , [B]
DO I=1,N
```

```
DO L=1,NL
LL=2*L
A(LL-1,L)=JN(I,L)
A(LL,L)=KL(L)*DJN(I,L)
IF(L.GT.1) THEN
A(LL-1,NL+L-1)=YN(I,L)
A(LL,NL+L-1)=KL(L)*DYN(I,L)
ENDIF
IF(L.LT.NL) THEN
A(LL-1,L+1)=-JN1(I,L)
A(LL,L+1)=-KL(L+1)*DJN1(I,L)
A(LL-1,NL+L)=-YN1(I,L)
A(LL,NL+L)=-KL(L+1)*DYN1(I,L)
ELSE
A(LL-1,NL+L)=-(JN1(I,L)-CI*YN1(I,L))
A(LL,NL+L)=-KL(L+1)*(DJN1(I,L)-CI*DYN1(I,L))
B(LL-1)=JN1(I,L)
B(LL)=KL(L+1)*DJN1(I,L)
ENDIF
ENDDO
CALL DSIMQ(A,B,2*NL,KS)
IF(KS.EQ.1) STOP
CM(2,1,I)=CZ
DO LR=1,NL
CM(1,LR,I)=B(LR)
CM(2,LR+1,I)=B(NL+LR)
B(LR)=CZ
B(NL+LR)=CZ
DO LC=1,2*NL
A(LR,LC)=CZ
A(NL+LR,LC)=CZ
ENDDO
ENDDO
TYPE *, I,CM(2,NL+1,I)
ENDDO
C
C COMPUTE BESSEL'S FUNCTIONS ALONG THE RADIUS
```

```
C
DO M=1,N
DO I=1,NP
JN(M,I)=0.D0
JN1(M,I)=0.D0
YN(M,I)=0.D0
YN1(M,I)=0.D0
ENDDO
ENDDO
CALL BES1(N,JN,KR1,NP1)
CALL BESSEL(N,JN1,YN1,KR2,NP2)
DO M=1,N
DO I=NP1+1,NP
JN(M,I)=JN1(M,I-NP1)
YN(M,I)=YN1(M,I-NP1)
ENDDO
ENDDO
C
C COMPUTE E-FIELD BY SUMMING THE TERMS OF FOURIER SE-
RIES
C
OPEN(UNIT=1,NAME='ANMCYL.DAT',TYPE='NEW')
L=NL+1
THE=PI
DO I=1,NP
J=NP-I+1
IF(L.NE.1 .AND. J.LE.NPOINT(L-1)) THEN
L=L-1
TYPE *, ' INTERFACE BETWEEN LAYERS',L+1, ' and',L
ENDIF
U=CM(1,L,1)*JN(1,J)+CM(2,L,1)*YN(1,J)
DO MM=2,N
PHI=CI*(MM-1)*(THE-PI/2.D0)
TERM=CM(1,L,MM)*JN(MM,J)+CM(2,L,MM)*YN(MM,J)
U=U+TERM*CDEXP(PHI)-(-1)**MM*TERM*CDEXP(-PHI)
C IF(J.EQ.1) TYPE 4, MM,JN(MM,J)
ENDDO
```

```
TYPE 4, J,R(J)*DCOS(THE)/RA(NL),CDABS(U)
WRITE(1,1) R(J)*DCOS(THE)/RA(NL),CDABS(U)
ENDDO
THE=0.D0
DO J=1,NP
IF(J.GT.NPOINT(L)) THEN
L=L+1
TYPE *, ' INTERFACE BETWEEN LAYERS',L-1, ' and',L
ENDIF
U=CM(1,L,1)*JN(1,J)+CM(2,L,1)*YN(1,J)
DO MM=2,N
PHI=CI*(MM-1)*(THE-PI/2.D0)
TERM=CM(1,L,MM)*JN(MM,J)+CM(2,L,MM)*YN(MM,J)
U=U+TERM*CDEXP(PHI)-(-1)**MM*TERM*CDEXP(-PHI)
ENDDO
TYPE 4, J,R(J)*DCOS(THE)/RA(NL),CDABS(U)
WRITE(1,1) R(J)*DCOS(THE)/RA(NL),CDABS(U)
ENDDO
WRITE(1,1) -999.D0,-999.D0
CLOSE(UNIT=1)
1 FORMAT(F10.2,F10.3)
2 FORMAT(/,' WAVELENGTH IN FREE SPACE IS',F10.3,' m',/, ' EN-
TER THE RADIUS OF THE CYLINDER [m]')
3 FORMAT(' Enter distance D [R] for plotting E-field line',/, ' and number
of points (odd)')
4 FORMAT(I8,F10.2,F10.3)
5 FORMAT(3X,'Enter Er1 ,Er2, Radius[Lamda0] and ', 'Number of points
for layer',I3)
STOP
END
C
C
SUBROUTINE BESSEL(N,Jn,Yn,X,K)
COMPLEX*16 Yn(20,300),Jn(20,300),X(300)
COMPLEX*16 CR,CI,SUM1,SUM2,SUM3,TERM,TERM3,A,XS,ARG
REAL*8 PI,GAMMA,FN,FN3,HI,HNI,HN
INTEGER SIGN
```

```
PI=4.D0*DATAN(1.D0)
GAMMA=0.5772156649D0
CR=DCMPLX(1.D0,0.D0)
DO NN=1,N
NB=NN-1
FN=1.D0
HN=0.D0
DO I=1,NB
FN=FN/I
HN=HN+1.D0/I
ENDDO
IF(NB.EQ.0) THEN
FN3=0.D0
ELSE
FN3=1.D0/(FN*NB)
ENDIF
ARG=CR*(PI/4.D0+NB*PI/2.D0)
DO J=1,K
XS=X(J)/2.D0
IF(CDABS(X(J)).GT.35.D0) THEN
Jn(NN,J)=CDCOS(X(J)-ARG)/CDSQRT(PI*XS)
Yn(NN,J)=CDSIN(X(J)-ARG)/CDSQRT(PI*XS)
ELSE
HI=0.D0
HNI=HN
SIGN=1
SUM1=CR*FN
SUM2=-CR*HN*FN
SUM3=CR*FN3
TERM=SUM1
TERM3=SUM3
A=XS**NB
I=0
100 I=I+1
HI=HI+1.D0/I
HNI=HNI+1.D0/(NB+I)
TERM=TERM/I*XS/(NB+I)*XS
```

```
SUM1=SUM1-SIGN*TERM
SUM2=SUM2+SIGN*TERM*(HI+HNI)
IF(I.LE.NB-1) THEN
TERM3=TERM3/I*XS/(NB-I)*XS
SUM3=SUM3+TERM3
ENDIF
SIGN=-SIGN
IF(CDABS(TERM).GT.1.D-20 .OR.
(I.LE.NB-1 .AND. CDABS(TERM3).GT.1.D-20)) GOTO 100
Jn(NN,J)=SUM1*A
Yn(NN,J)=2.D0/PI*(Jn(NN,J)*(CDLOG(XS)+CR*GAMMA)
+0.5D0*(A*SUM2-SUM3/A))
ENDIF
ENDDO
ENDDO
RETURN
END
C
C
SUBROUTINE BES1(N,Jn,X,K)
COMPLEX*16 Jn(20,300),X(300),CR,SUM1,A,XS,TERM
REAL*8 PI,GAMMA,FN
INTEGER SIGN
PI=4.D0*DATAN(1.D0)
GAMMA=0.5772156649D0
CR=DCMPLX(1.D0,0.D0)
DO NN=1,N
NB=NN-1
FN=1.D0
DO I=1,NB
FN=FN/I
ENDDO
DO J=1,K
XS=X(J)/2.D0
IF(CDABS(X(J)).GT.35.D0) THEN
Jn(NN,J)=CDSQRT(1.D0/PI/XS) *CDCOS(X(J)
-CR*(PI/4.D0+NB*PI/2.D0))
```

```
ELSE
SIGN=1
IF(NB.EQ.0) THEN
A=CR
ELSE
A=XS**NB
ENDIF
SUM1=CR*FN
TERM=CR*FN
I=0
100 I=I+1
TERM=TERM/I*XS/(NB+I)*XS
SUM1=SUM1-SIGN*TERM
SIGN=-SIGN
IF(CDABS(TERM).GT.1.D-20) GOTO 100
Jn(NN,J)=A*SUM1
ENDIF
ENDDO
ENDDO
RETURN
END
C*********
C SUBROUTINE DSIMQ
C********

   SUBROUTINE DSIMQ(A,B,N,KS)
DIMENSION A(*),B(*)
COMPLEX*16 A,B,BIGA,SAVE,CZ
REAL*8 TOL
C—
CZ=DCMPLX(0.D0,0.D0)
TOL=0.D0
KS=0
JJ=-N
DO 65 J=1,N
JY=J+1
JJ=JJ+N+1
```

```
BIGA=CZ
IT=JJ-J
DO 30 I=J,N
IJ=IT+I
IF(CDABS(A(IJ)) .GT. CDABS(BIGA)) THEN
BIGA=A(IJ)
IMAX=I
ENDIF
30 CONTINUE
IF (CDABS(BIGA)-TOL) 35,35,40
35 KS=1
RETURN
C---
40 I1=J+N*(J-2)
IT=IMAX-J
DO 50 K=J,N
I1=I1+N
I2=I1+IT
SAVE=A(I1)
A(I1)=A(I2)
A(I2)=SAVE
50 A(I1)=A(I1)/BIGA
SAVE=B(IMAX)
B(IMAX)=B(J)
B(J)=SAVE/BIGA
C---
IF(J-N) 55,70,55
55 IQS=N*(J-1)
DO 65 IX=JY,N
IXJ=IQS+IX
IT=J-IX
DO 60 JX=JY,N
IXJX=N*(JX-1)+IX
JJX=IXJX+IT
60 A(IXJX)=A(IXJX)-(A(IXJ)*A(JJX))
65 B(IX)=B(IX)-(B(J)*A(IXJ))
C---
```

```
70 NY=N-1
IT=N*N
DO 80 J=1,NY
IA=IT-J
IB=N-J
IC=N
DO 80 K=1,J
B(IB)=B(IB)-A(IA)*B(IC)
IA=IA-N
80 IC=IC-1
RETURN
END
```

Appendix E

Computer Program for Multi-layered Circular Cylinder of Lossy Dispersive Media Exposed to a Continuous Plane Wave. The FDTD Solution.

```
THIS PROGRAM CALCULATES E-FIELD FOR A DISPERSIVE DIELEC-
TRIC MULTILAYER CIRCULAR CYLINDER OF INFINITE LENGTH
EXPOSED TO A NORMALLY INCIDENT PLANE WAVE PULSE US-
ING TDFD METHOD. CASE (E-FIELD // Z-AXIS)
C
REAL*8 EZ(200,400),HX(200,400),HY(200,400),EMAX(200,400)
REAL*8 EZ0(200,400),SUM(200,400)
REAL*8 AXN(3,400),AYP(2,200,3),AYN(200,3)
REAL*8 MU0,EPS0,NU0,V0,LAMDA0
REAL*8 ER(5),ERS(5),ES(5),ESS(5),W0(5),S(5),W0DT(5)
REAL*8 QEE(5),QEH(5),QES(5),RA(5),G(5)
REAL*8 EI,PI,ALPHA,P,QH,RTX,DIST,RADI,LAMDA,A
REAL*8 FREQ,W,T,DT,DR,R,OX,OY,V
```

```
CHARACTER*20 MORE, FNAME
C
R(I,J,OX,OY,DR)=DR*DSQRT((I-OX)**2+(J-OY)**2)
PI=4.D0*DATAN(1.D0)
MU0=4.D-7*PI
V0=2.997925D8
EPS0=1.D0/(V0*V0*MU0)
NU0=DSQRT(MU0/EPS0)
FREQ=2.5D9
W=2.D0*PI*FREQ
LAMDA0=V0/FREQ
P=0.5D0
TYPE *, ' WAVELENGTH IN FREE SPACE IS',LAMDA0
TYPE *, ' ENTER NUMBER OF LAYERS AND NUMBER OF SEG-
MENTS ALONG THE RADIUS'
ACCEPT *, NL,NR
T=0.D0
DO L=1,NL
TYPE 5, L
ACCEPT *, ES(L),ER(L),W0(L),S(L),RA(L)
ESS(L)=EPS0*ES(L)
ERS(L)=EPS0*ER(L)
RA(L)=LAMDA0*RA(L)
V=V0/DSQRT(ER(L))
IF(L.EQ.1) THEN
T=T+RA(L)/V
ELSE
T=T+(RA(L)-RA(L-1))/V
ENDIF
ENDDO
RA(NL+1)=1.D10
DR=RA(NL)/NR
DT=P*DR/V0
TYPE *, ' PERIOD IS', INT(T/DT)
NT=INT(T/DT)
TYPE *, ' TIME WINDOW IS',INT(6.D0*T/DT)
RTX=DT/DR
```

```
DO L=1,NL
W0DT(L)=W0(L)*DT
A=(ES(L)-ER(L))/ER(L)
QEE(L)=1.D0-DT*S(L)/ERS(L)-A*W0DT(L)
QEH(L)=RTX/ERS(L)
QES(L)=A*W0DT(L)**2
G(L)=DEXP(-W0DT(L))
ENDDO
QEE(NL+1)=1.D0
QEH(NL+1)=RTX/EPS0
QES(NL+1)=0.D0
W0DT(NL+1)=1.D0
QH=RTX/MU0
TYPE *, ' ENTER IMAX, JMAX and NMAX'
ACCEPT *, IMAX,JMAX,NMAX
OX=IMAX+0.5D0
OY=JMAX/2+0.5D0
TYPE *, ' ENTER J FOR THE EXCITATION LINE'
ACCEPT *, JEX
DO N=1,NMAX
EI=DSIN(W*N*DT)
C
C LINE OF EXCITATION
C
DO I=2,IMAX+1
EZ(I,JEX)=EZ(I,JEX)+EI
ENDDO
C
C ABSORBING BOUNDARY
C
DO J=2,JMAX
HY(1,J)=HY(1,J)+QH*(EZ(2,J)-EZ(1,J))
EZ(1,J)=EZ(1,J)+EZ(2,J)-AXN(2,J)
+P*(EZ(2,J)-EZ(1,J)-(AXN(3,J)-AXN(2,J)))
ENDDO
DO I=2,IMAX
HX(I,1)=HX(I,1)-QH*(EZ(I,2)-EZ(I,1))
```

```
EZ(I,1)=EZ(I,1)+EZ(I,2)-AYN(I,2)
+P*(EZ(I,2)-EZ(I,1)-(AYN(I,3)-AYN(I,2)))
ENDDO
DO K=1,3
DO J=2,JMAX
AXN(K,J)=EZ(K,J)
ENDDO
DO I=2,IMAX
AYN(I,K)=EZ(I,K)
ENDDO
ENDDO
EZ(1,1)=EZ(1,1)+P*(EZ(2,2)-EZ(1,1))
EZ(1,JMAX+1)=EZ(1,JMAX+1)+P*(EZ(2,JMAX)-EZ(1,JMAX+1))
C
C COMPUTE THE FIELDS FOR I=2,IMAX and J=2,JMAX
C
MOVING=N+1
IF(MOVING.GT.JMAX) MOVING=JMAX
DO I=2,IMAX
DO J=2,MOVING
RADI=R(I,J,OX,OY,DR)
L=0
20 L=L+1
IF(RADI.GT.RA(L)) GOTO 20
HX(I,J)=HX(I,J)-QH*(EZ(I,J+1)-EZ(I,J))
HY(I,J)=HY(I,J)+QH*(EZ(I+1,J)-EZ(I,J))
EZ(I,J)=QEE(L)*EZ(I,J)+QES(L)*SUM(I,J)
+QEH(L)*((HY(I,J)-HY(I-1,J))-(HX(I,J)-HX(I,J-1)))
SUM(I,J)=G(L)*SUM(I,J)+(EZ(I,J)+G(L)*EZ0(I,J))/2.D0
IF(I.EQ.IMAX) EZ(IMAX+1,J)=EZ(IMAX,J)
IF(N.GE.(NMAX-NT/2) .AND. DABS(EZ(I,J)).GT.EMAX(I,J))
EMAX(I,J)=DABS(EZ(I,J))
ENDDO
ENDDO
DO I=2,IMAX
EZ(I,JMAX+1)=EZ(I,JMAX+1)+AYP(1,I,2)-AYP(2,I,2)
+P*(AYP(1,I,2)-EZ(I,JMAX+1)-(AYP(2,I,3)-AYP(2,I,2)))
```

```
ENDDO
DO K=1,3
DO I=2,IMAX
JM=JMAX+2-K
AYP(2,I,K)=AYP(1,I,K)
AYP(1,I,K)=EZ(I,JM)
ENDDO
ENDDO
EZ(IMAX+1,1)=EZ(IMAX,1)
EZ(IMAX+1,JMAX+1)=EZ(IMAX,JMAX+1)
JUMPI=(IMAX)/10+1
JUMPJ=(JMAX)/22+1
IF(MOD(N,50).EQ.0) THEN
TYPE 4, N,(I,I=1,IMAX+1,JUMPI)
DO J=1,JMAX+1,JUMPJ
TYPE 3, J,(EZ(I,J),I=1,IMAX+1,JUMPI)
ENDDO
ENDIF
DO I=1,IMAX+1
DO J=1,JMAX+1
EZ0(I,J)=EZ(I,J)
ENDDO
ENDDO
C
ENDDO
C
10 TYPE *, ' ENTER DISTANCE [R] FROM CENTER FOR E-FIELD-
LINE PLOTTED'
ACCEPT *, DIST
DIST=DIST*RA(NL)/DR
IP=IMAX-INT(DIST)
JR=INT(DSQRT((RA(NL)/DR)**2-DIST**2))
JB=JMAX/2-JR+1
JE=JMAX/2+JR
TYPE *, IP,JB,JE
TYPE *, ' ENTER FILE NAME'
ACCEPT 2, FNAME
```

```
OPEN(UNIT=1,NAME=FNAME,TYPE='NEW')
TYPE 1, ((J-OY)/NR,EMAX(IP,J),J=JB,JE)
WRITE(1,1) ((J-OY)/NR,EMAX(IP,J),J=JB,JE)
WRITE(1,1) -999.D0, -999.D0
CLOSE(UNIT=1)
TYPE *, ' WANT ANOTHER FILE ? [Y/N]'
ACCEPT 2, MORE
IF(MORE.EQ.'Y') GOTO 10
1 FORMAT(2(F10.3))
2 FORMAT(A20)
3 FORMAT(I4,10(F7.3))
4 FORMAT(//,5X,'N =',I5,/,4X,10(I7))
5 FORMAT(/, ' ENTER ES, ER, W0, S, AND' ' RADIUS[LAMDA0] FOR
LAYER',I3)
STOP
END
```

Appendix F

Computer Program for Multi-layered Circular Cylinder of Lossy Dispersive Media Exposed to a Pulsed Plane Wave. The FDTD Solution.

```
THIS PROGRAM CALCULATES E-FIELD FOR A DISPERSIVE DIELEC-
TRIC MULTILAYER CIRCULAR CYLINDER OF INFINITE LENGTH
EXPOSED TO A NORMALLY INCIDENT PLANE WAVE PULSE US-
ING TDFD METHOD. CASE (E-FIELD // Z-AXIS)
C
REAL*8 EZ(200,400),HX(200,400),HY(200,400)
REAL*8 EZ0(200,400),SUM(200,400),EPLOT(200,400)
REAL*8 AXN(3,400),AYP(2,200,3),AYN(200,3)
REAL*8 MU0,EPS0,NU0,V0
REAL*8 ER(5),ERS(5),ES(5),ESS(5),W0(5),S(5),W0DT(5)
REAL*8 QEE(5),QEH(5),QES(5),RA(5),G(5)
REAL*8 EI,PI,ALPHA,P,QH,RTX,DIST,RADI,LAMDA,A
REAL*8 T1,T,DT,DR,R,OX,OY,V
```

```
INTEGER NPLOT(5)
CHARACTER*20 MORE, FNAME
C
C RADIUS OF THE CYLINDER AS A FUNCTION OF I and J
C
R(I,J,OX,OY,DR)=DR*DSQRT((I-OX)**2+(J-OY)**2)
C
PI=4.D0*DATAN(1.D0)
MU0=4.D-7*PI
V0=2.997925D8
EPS0=1.D0/(V0*V0*MU0)
NU0=DSQRT(MU0/EPS0)
P=0.5D0
C
C DATA INPUT
C
TYPE *, ' ENTER NUMBER OF LAYERS AND NUMBER OF SEG-
MENTS ALONG THE RADIUS'
ACCEPT *, NL,NR
T=0.D0
DO L=1,NL
TYPE 5, L
ACCEPT *, ES(L),ER(L),W0(L),S(L),RA(L)
ESS(L)=EPS0*ES(L)
ERS(L)=EPS0*ER(L)
V=V0/DSQRT(ER(L))
IF(L.EQ.1) THEN
T=T+RA(L)/V
ELSE
T=T+(RA(L)-RA(L-1))/V
ENDIF
ENDDO
RA(NL+1)=1.D10
DR=RA(NL)/NR
DT=P*DR/V0
NT=INT(T/DT)
TYPE *, ' TIME STEP IS',DT
```

```
TYPE *, ' PROPAGATION TIME IS',INT(2.D0*T/DT)
TYPE *, ' ENTER NUMBER OF SNAPSHOTS'
ACCEPT *, NSNAP
DO LLL=1,NSNAP
TYPE *, ' ENTER TIME TO PLOT SNAPSHOT',LLL
ACCEPT *, NPLOT(LLL)
ENDDO
RTX=DT/DR
C
C CALCULATIONS OF NECESSARY COEFFICIENTS FOR THE ITER-
ATION
C
DO L=1,NL
W0DT(L)=W0(L)*DT
A=(ES(L)-ER(L))/ER(L)
QEE(L)=1.D0-DT*S(L)/ERS(L)-A*W0DT(L)
QEH(L)=RTX/ERS(L)
QES(L)=A*W0DT(L)**2
G(L)=DEXP(-W0DT(L))
ENDDO
QEE(NL+1)=1.D0
QEH(NL+1)=RTX/EPS0
QES(NL+1)=0.D0
W0DT(NL+1)=1.D0
QH=RTX/MU0
C
C SET THE GRID SIZE, NUMBER OF TIME STEPS AND EXCITATION
LINE
C
TYPE *, ' ENTER IMAX, JMAX and NMAX'
ACCEPT *, IMAX,JMAX,NMAX
OX=IMAX+0.5D0
OY=JMAX/2+0.5D0
TYPE *, ' ENTER J FOR THE EXCITATION LINE'
ACCEPT *, JEX
C
C SET INITIAL TIME FOR GAUSSIAN PULSE ONLY
```

```
C
T1=20.D-11
T=-80.D-11
C
LSN=1
DO N=1,NMAX
T=T+DT
C
C INCIDENT PULSE (EMP OR GAUSSIAN PULSE)
C
C EI=1.05016D0*(DEXP(-4.D6*T)-DEXP(-4.76D8*T))
EI=DEXP(-(T/T1)**2/2.D0)
C
C LINE OF EXCITATION
C
DO I=2,IMAX+1
EZ(I,JEX)=EZ(I,JEX)+EI
ENDDO
C
C ABSORBING BOUNDARY CONDITIONS
C
DO J=2,JMAX
HY(1,J)=HY(1,J)+QH*(EZ(2,J)-EZ(1,J))
EZ(1,J)=EZ(1,J)+EZ(2,J)-AXN(2,J)
+P*(EZ(2,J)-EZ(1,J)-(AXN(3,J)-AXN(2,J)))
ENDDO
DO I=2,IMAX
HX(I,1)=HX(I,1)-QH*(EZ(I,2)-EZ(I,1))
EZ(I,1)=EZ(I,1)+EZ(I,2)-AYN(I,2)
+P*(EZ(I,2)-EZ(I,1)-(AYN(I,3)-AYN(I,2)))
ENDDO
DO K=1,3
DO J=2,JMAX
AXN(K,J)=EZ(K,J)
ENDDO
DO I=2,IMAX
AYN(I,K)=EZ(I,K)
```

```
ENDDO
ENDDO
EZ(1,1)=EZ(1,1)+P*(EZ(2,2)-EZ(1,1))
EZ(1,JMAX+1)=EZ(1,JMAX+1)+P*(EZ(2,JMAX)-EZ(1,JMAX+1))
C
C COMPUTE THE FIELDS FOR I=2,IMAX and J=2,JMAX
C
MOVING=N+1
IF(MOVING.GT.JMAX) MOVING=JMAX
DO I=2,IMAX
DO J=2,MOVING
C
C SEARCH FOR THE LAYER OF THE CALCULATING POINT
C
RADI=R(I,J,OX,OY,DR)
L=0
20 L=L+1
IF(RADI.GT.RA(L)) GOTO 20
C
HX(I,J)=HX(I,J)-QH*(EZ(I,J+1)-EZ(I,J))
HY(I,J)=HY(I,J)+QH*(EZ(I+1,J)-EZ(I,J))
EZ(I,J)=QEE(L)*EZ(I,J)+QES(L)*SUM(I,J)
+QEH(L)*((HY(I,J)-HY(I-1,J))-(HX(I,J)-HX(I,J-1)))
SUM(I,J)=G(L)*SUM(I,J)+(EZ(I,J)+G(L)*EZ0(I,J))/2.D0
IF(I.EQ.IMAX) EZ(IMAX+1,J)=EZ(IMAX,J)
IF(N.EQ.NPLOT(LSN)) EPLOT(I,J)=EZ(I,J)
ENDDO
ENDDO
C
C ABSORBING BOUNDARY CONDITIONS
C
DO I=2,IMAX
EZ(I,JMAX+1)=EZ(I,JMAX+1)+AYP(1,I,2)-AYP(2,I,2)
+P*(AYP(1,I,2)-EZ(I,JMAX+1)-(AYP(2,I,3)-AYP(2,I,2)))
ENDDO
DO K=1,3
DO I=2,IMAX
```

```
JM=JMAX+2-K
AYP(2,I,K)=AYP(1,I,K)
AYP(1,I,K)=EZ(I,JM)
ENDDO
ENDDO
EZ(IMAX+1,1)=EZ(IMAX,1)
EZ(IMAX+1,JMAX+1)=EZ(IMAX,JMAX+1)
JUMPI=(IMAX)/10+1
JUMPJ=(JMAX)/22+1
IF(MOD(N,50).EQ.0) THEN
TYPE 4, N,T,(I,I=1,IMAX+1,JUMPI)
DO J=1,JMAX+1,JUMPJ
TYPE 3, J,(EZ(I,J),I=1,IMAX+1,JUMPI)
ENDDO
ENDIF
DO I=1,IMAX+1
DO J=1,JMAX+1
EZ0(I,J)=EZ(I,J)
ENDDO
ENDDO
C
IF(N.EQ.NPLOT(LSN)) THEN
LSN=LSN+1
10 TYPE *, ' ENTER DISTANCE [R] FROM CENTER ', 'FOR E-FIELD-
LINE PLOTTED'
ACCEPT *, DIST
DIST=DIST*RA(NL)/DR
IP=IMAX-INT(DIST)
JR=INT(DSQRT((RA(NL)/DR)**2-DIST**2))
JB=JMAX/2-JR+1
JE=JMAX/2+JR
TYPE *, IP,JB,JE
TYPE *, ' ENTER FILE NAME'
ACCEPT 2, FNAME
OPEN(UNIT=1,NAME=FNAME,TYPE='NEW')
TYPE 1, ((J-OY)/NR,EPLOT(IP,J),J=JB,JE)
WRITE(1,1) ((J-OY)/NR,EPLOT(IP,J),J=JB,JE)
```

```
WRITE(1,1) -999.D0, -999.D0
CLOSE(UNIT=1)
TYPE *, ' WANT ANOTHER FILE ? [Y/N]'
ACCEPT 2, MORE
IF(MORE.EQ.'Y') GOTO 10
ENDIF
ENDDO
C
1 FORMAT(2(F10.3))
2 FORMAT(A20)
3 FORMAT(I4,10(F7.3))
4 FORMAT(//,5X,'N =',I5,' T =',E9.2,/,4X,10(I7))
5 FORMAT(/, ' Enter ES, ER, W0, S, &' ' Radius [m] for layer',I3)
STOP
END
```

Appendix G

Previously Obtained Results

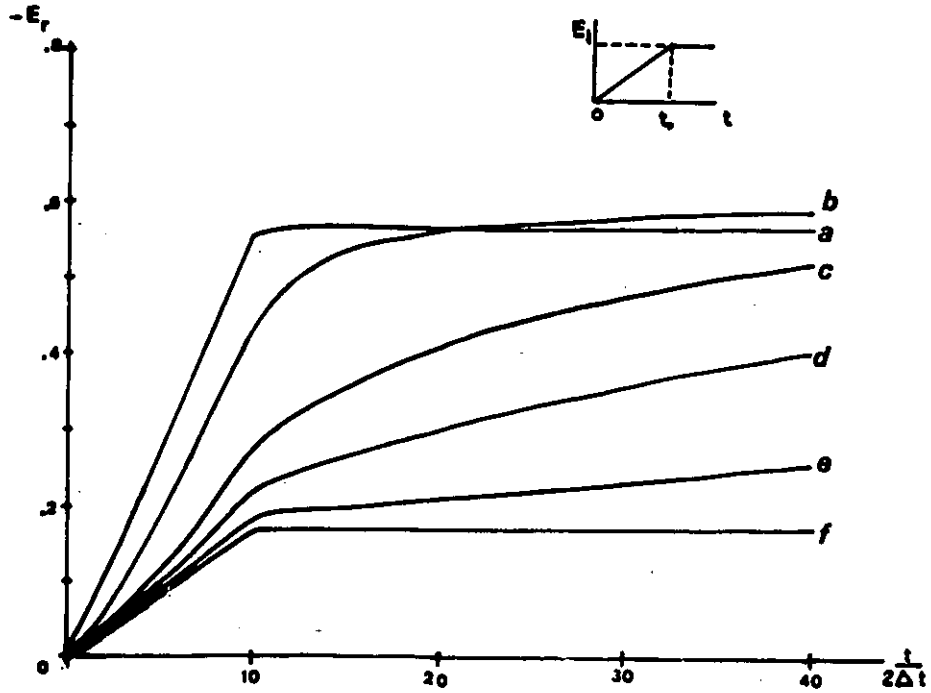

Reflected field at the interface of a Debye medium illuminated by a ramp incident field: $\epsilon_r = 2$, $\epsilon_s = 13$, $1/\omega_0 \approx 10^{-9}$s, $\sigma = 0$. (a) $\omega_0 \Delta t \geq 1.5$. (b) $\omega_0 \Delta t = 10^{-1}$. (c) $\omega_0 \Delta t = 2.10^{-2}$. (d) $\omega_0 \Delta t = 8.10^{-3}$. (e) $\omega_0 \Delta t = 2.10^{-3}$. (f) $\omega_0 \Delta t \leq 10^{-6}$.

Figure G.1: Results obtained by Bolomey.

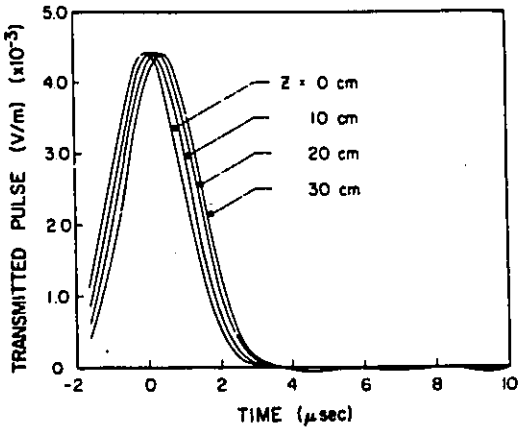

Transmitted waveforms of Gaussian incident pulse as a function of time and depth for $t_1 = 1\ \mu s$.

Figure G.2: Results obtained by Lin.

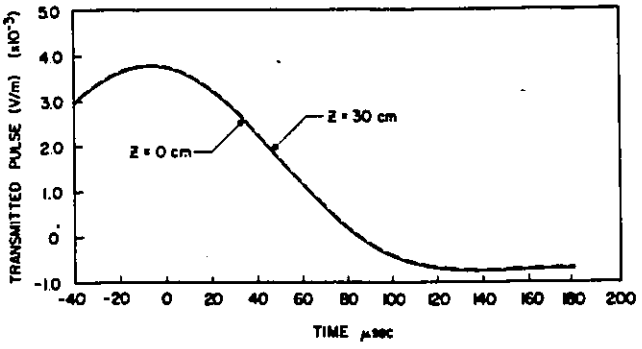

Transmitted waveforms of Gaussian incident pulse as a function of time and depth for $t_1 = 50\ \mu s$.

Figure G.3: Results obtained by Lin.

Bibliography

[1] Carl H. Durney, *Electromagnetic Dosimetry for Models of Humans and Animals: A Review of Theoretical and Numerical Techniques,* Proc. IEEE, Vol. 68, No. 1, pp. 33-40, January 1980.

[2] Sol M. Michaelson, *Microwave Biological Effects: An Overview,* Proc. IEEE, Vol. 68, No. 1, pp. 40-49, January 1980.

[3] A.W. Guy, *A Note on EMP Safety Hazards,* IEEE Trans. on Biomed. Eng., Vol. BME-22, No. 6, pp. 464-467, November 1975.

[4] J. A. Fuller and J. R. Wait, *Electromagnetic Pulse Transmission in Homogeneous Dispersive Rock,* IEEE Trans. on Ant. & Prop., Vol. AP-20, pp 530-533, July 1972.

[5] R.W.P. King and C.W. Harrison,Jr., *The Transmission of Electromagnetic Waves and Pulses into the Earth,* J. Applied Physics, Vol. 39, No. 9, pp. 4444-4452, August 1968.

[6] T. Suzuki, E. Ogawa and H. Fujioka, *Reflection of Pulse by Multiple-Dielectric Layers,* IEEE Trans. on Ant. & Prop., pp. 127-129, January 1975.

[7] T.M. Papazoglou, *Transmission of a Transient Electromagnetic Plane Wave into a Lossy Half Space,* J. Appl. Phys., Vol. 46, No. 8, pp. 3333-3341, August 1975.

[8] J. R. Wait, *Propagation of Pulses in Dispersive Media,* Radio Science, Journal of Research NBS/USNC-URSI, Vol. 69D, pp 1387-1401, November 1965.

[9] R. Sivaprasad, K. C. Stotz, and N. N. Susungi, *Reflection of Pulses at Oblique Incidence from Stratified Dispersive Media*, IEEE Trans. on Ant. & Prop., pp 95-99, January 1976.

[10] H.E. Bussey and J.H. Richmond, *Scattering by a Lossy Dielectric Circular Cylindrical Multilayer, Numerical Values*, IEEE Trans. on Ant. & Prop., pp. 723-725, September 1975.

[11] J. C. Lin, *Interaction of Electromagnetic Transient Radiation with Biological Materials*, IEEE Trans. on EMC, Vol. EMC-17, No 2, pp. 93-97, May 1975.

[12] J.C. Lin, C.L. Wu and C.K. Lam, *Transmission of Electromagnetic Pulse into the Head*, Proc. IEEE, pp 1726-1727, December 1975.

[13] James C. Lin, *Electromagnetic Pulse Interaction with Mammalian Cranial Structures*, IEEE Trans. on Biomed. Eng., Vol. BME-23, No. 1, pp. 61-65, January 1976.

[14] C. H. Durney, T. G. Stockham, Jr., and K. Moten, *Electromagnetic Pulse Propagation*, Elect. Eng. Dept., Univ. of Utah, Tech. Rep. A-3529-240, February 1987.

[15] K. Moten, C.H. Durney and T.G. Stockham, Jr., *Electromagnetic Pulse Propagation in Dispersive Planar Dielectrics*, Bioelectromagnetics 10, pp. 35-49, 1989.

[16] Dong Hoa Lam, *Finite Difference Method for Transient Signal Propagation in Stratified Dispersive Media*, Electroscience Lab., Ohio State Univ., Columbus, Tech. Rep. 3892-1, January 1975.

[17] J. Ch. Bolomey, Ch. Durix, and D. Lesselier, *Time Domain Integral Equation Approach for Inhomogeneous and Dispersive Slab Problem*, IEEE Trans. on Ant. & Prop., Vol. AP-26, No 5, pp 658-667, September 1978.

[18] R. Holland, L. Simpson and K.S. Kunz, *Finite-Difference Analysis of EMP Coupling to Lossy Dielectric Structures*, IEEE trans. on EMC, Vol. EMC-22, No. 3, pp. 203-209, August 1980.

[19] D.M. Sullivan, D.T. Borup and O.P. Gandhi, *Use of the Finite-Difference Time-Domain Method in Calculating EM Absorption in Human Tissues,* IEEE Trans. on Biomed. Eng., Vol. BME-34, No. 2, pp. 148-157, February 1987.

[20] C. C. Lin, *Numerical Modeling of Two-Dimensional Time Domain Electromagnetic Scattering by Underground Inhomogeneities,* Ph.D. Dissertation, Dept. EECS, Univ. Calif., Berkely, CA, 1985.

[21] A. Taflove and M.E. Brodwin, *Numerical Solution of Steady-State Electromagnetic Scattering Problems Using the Time-Dependent Maxwell's Equations,* IEEE Trans. on Microwave Theory & Tech., Vol. MTT-23, No. 8, pp. 623-630, August 1975.

[22] K.S. Yee, *Numerical Solution of Initial Boundary Value Problems Involving Maxwell's Equations in Isotropic Media,* IEEE Trans. on Ant. & Prop., Vol. AP-14, No. 3, pp. 302-307, May 1966.

[23] S. I Hariharan, *Absorbing Boundary Conditions for Exterior Problems,* NASA CR-177944, July 1985.

[24] G. Mur, *Absorbing Boundary Conditions for the Finite-Difference Approximation of the Time-Domain Electromagnetic-field Equations,* IEEE Trans. on EMC, Vol. EMC-23, No. 4, pp. 377-382, November 1981.

[25] B. Engquist and A. Majda, *Absorbing Boundary Conditions for the Numerical Simulation of Waves,* Math. Comp., Vol. 31, No. 139, pp. 629-651, July 1977.

[26] A.C. Reynolds, *Boundary Conditions for the Numerical Solution of Wave Propagation Problems,* J. Physics, Vol. 43, No. 6, pp. 1099-1110, October 1978.

[27] C.D. Taylor, D.H. Lam and T.H. Shumpert, *Electromagnetic Pulse Scattering in Time-Varying Inhomogeneous Media,* IEEE trans. on Ant. & Prop., Vol. AP-17, No. 5, pp. 585-589, September 1969.

[28] S.S. Stuchly, M.A. Rzepecka and M.F. Iskander, *Permittivity Measurements at Microwave Frequencies Using Lumped Elements,* IEEE Trans. on Ins. & Meas., Vol. IM-23, No. 1, pp. 56-62, March 1974.

[29] A. Kraszewski, S.S. Stuchly, M.A. Stuchly and S.A. Symons, *On the Measurement Accuracy of the Tissue Permittivity in Vivo,* IEEE Trans. on Ins. & Meas., Vol. IM-32, No. 1, pp. 37-42, March 1983.

[30] D. Arnush, *Electromagnetic Pulse (EMP) Propagation Through an Absorptive and Dispersive Medium,* IEEE Trans. on Ant. & Prop., Vol. AP-23, No. 5, pp. 623-626, September 1975.

[31] N.E. Hill *et al, Dielectric Properties and Molecular Behavior,* Van Nostrand Reinhold, New York, 1969.

[32] M.A. Stuchly and S.S. Stuchly, *Dielectric Properties of Biological Substances - Tabulated,* J. Microwave Power, Vol. 15, pp. 19-26, 1980.

[33] A.V. Oppenheim *et al, Signals and Systems,* Prentice-Hall, pp 223-225, Toronto, 1983.

[34] L.C. Shen and J.A. Kong, *Applied Electromagnetism,* Brooks/Cole Engineering Division, Wadsworth Inc., pp 18-64, Cali., 1983.

[35] C.A. Balanis, *Antenna Theory Analysis and Design,* Harper & Row, pp 755-766, New York, 1982.

[36] E. Kreyszig, *Advanced Engineering Mathematics,* John Wiley & Sons Inc., pp 173-179, Toronto, 1983.

[37] R. Sherman *et al, EMP Engineering and Design Principles,* Bell Laboratories, Electrical Protection Department, Loop Transmission Division, pp 13, New Jersey, 1975.

[38] A. Taflove, *Review of the Formulation and Applications of the Finite-Difference Time-Domain Method for Numerical Modeling of Electromagnetic Wave Interactions with Arbitrary Structures,* Wave Motion, Vol. 10, pp 547-582, 1988.